MODELS FOR EVALUATION AND OPTIMIZATION OF GRID-SCALE ENERGY STORAGE IN PRESENCE OF RENEWABLE ENERGY

By

Atri Bera

A DISSERTATION

Submitted to
Michigan State University
in partial fulfillment of the requirements
for the degree of

Electrical Engineering – Doctor of Philosophy

2021

ABSTRACT

MODELS FOR EVALUATION AND OPTIMIZATION OF GRID-SCALE ENERGY STORAGE IN PRESENCE OF RENEWABLE ENERGY

By

Atri Bera

Power grids across the world are undergoing remarkable changes in recent times fueled by the extensive integration of renewable energy resources (RERs). While it has been well established that RERs help to alleviate environmental concerns, the high penetration of these resources poses some serious challenges to the reliability and stability of the power grid due to their intermittent nature and low-inertia characteristics. Energy storage systems (ESSs) can provide effective solutions to the aforementioned problems. These devices are well suited for providing multiple services to the power grid due to their flexibility in operation, high ramp rates, and decreasing costs. This work investigates the role of ESSs in alleviating the critical issues concerning the power grid in recent times and the economic viability of such solutions. First, a novel analytical approach is developed for sizing ESSs to maintain grid frequency stability by providing inertial support. This approach provides a solution to the problem of reduced inertia in a system with high penetration of RERs, which may lead to frequency stability issues or blackouts in more severe cases. A comprehensive investment planning framework for ESS projects is also developed, which can estimate the lifetime revenue of ESSs participating in market services while considering battery degradation. A new planning strategy is then presented, which brings together the technical and economic aspects of deploying ESSs for providing inertial support to the grid. This techno-economic framework is capable of optimally sizing ESSs for providing inertial support to the grid while minimizing the operational costs of the system by participating in electricity markets. Besides considering the stability issues of the modern power grid, the depleting reliability of the system due to high RER penetration is also considered in this work. A transmission planning approach is developed for this purpose, which can reduce the variability of wind power and enhance the reliability of wind-integrated systems by jointly utilizing ESSs and wind power aggregation.

To my parents.

ACKNOWLEDGMENTS

First and foremost, I would like to express my sincere gratitude to my advisor, Dr. Joydeep Mitra. The past five years under his tutelage has been a life-changing experience for me. Besides guiding me on the path to become an independent researcher, he has also taught me the skills necessary to navigate life in general. He has pushed me to become a better version of myself every single day. I have, and will always look up to him as a father figure. I cannot explain in words how much he has contributed to my life. All I can say is that I have been extremely fortunate to have him as my advisor, and I would not have it any other way.

I would also like to thank the members of my Ph.D. committee, Dr. Elias Strangas, Dr. Kalyanmoy Deb, and Dr. Ranjan Mukherjee. Their guidance and valuable feedback have helped me immensely in improving my work.

I would like to thank my colleagues from the **E**nergy **R**el**i**ability and **Se**curity (**ERiSe**) Lab, Dr. Nga Nguyen, Dr. Yuting Tian, Dr. Saleh Almasabi, Mr. Fares Alharbi, Mr. Khalil Sinjari, and Mr. Saad Alzahrani for their kind support and friendship. It was an honor working with such talented and humble people.

I would also like to thank my collaborators, Dr. Babu Chalamala, Dr. Ray Byrne, Dr. Tu Nguyen, Dr. Mohammed Ben-idris, and Dr. Anurag Chowdhury. I have enjoyed every moment of working with them and look forward to continue collaborating with them in the future.

Last but not least, I would like to thank my parents, friends, and family for their unconditional love, encouragement, patience, and compassion. They have always been by my side, partaking in all my happiness, and absorbing all my grievances with a smile on their faces. I could not have done this without them.

TABLE OF CONTENTS

LIST OF TABLES

LIST OF FIGURES

CHAPTER 1

INTRODUCTION

The share of energy consumption originating from fossil fuels like coal, natural gas, and petroleum is falling steadily across the globe due to their environmental impact leading to climate change. The limited nature of these resources also plays a part in the global drive to find alternative and more sustainable energy sources. Renewable energy resources (RERs), like wind and solar, are suitable candidates for this role due to their abundance, environmental benefits, and low costs of generation. In addition, sustained policy support and economic incentives for RERs across the world have led to their exponential growth in recent times. Electricity generation is not exempt from this growing trend and consequently, RERs have become key elements of the modern electric power grid. According to [1], wind and solar combined are projected to become the largest source of electricity generation in the world by 2025. The total installed wind power capacity in the U.S was 105 GW by the end of 2019 [2], with 65 GW more expected to be added by the end of 2020, despite the ongoing pandemic, while the expected global solar PV additions for 2020 was nearly 107 GW, representing an 18% growth from 2019 [1].

While the environmental benefits of RERs are well established, high penetration of these resources introduces uncertainties into the system and poses serious challenges to the reliability and stability of the power grid. This happens due to their intermittent nature and low-inertia characteristics. Energy storage systems (ESSs) can be used to provide effective solutions in the face of such uncertainty. These devices are well-suited for providing multiple services to the power grid due to their operational flexibility, high ramp rates, and decreasing costs. They can be deployed for applications like energy arbitrage, frequency regulation, inertial support, and firming up of RERs, among others. This thesis identifies the various problems associated with RER penetration into the power grid, investigates the role of ESSs in alleviating these issues, and develops models and frameworks for providing effective engineering solutions to these problems.

1.1 Motivation and Challenges

Conventional synchronous generators are dispatchable in nature and the operator has a high degree of control over its operation. In addition, these generators have high rotating masses, which can store large amounts of kinetic energy and provide the power grid with inertial support when an imbalance occurs in the system. However, in recent times, an increasing number of conventional generators are being replaced by RERs due to the reasons discussed above. Inverter-based resources are incapable of providing any mechanical inertial response and are thus unable to support frequency stability of the grid [3, 4]. Several studies have shown that the replacement of conventional generators with RERs causes reduction of system inertia, which leads to an increased rate of change of frequency (RoCoF) and lower frequency nadirs [5, 6]. Independent system operators like Electric Reliability Council of Texas (ERCOT) [7] and regulatory bodies like North American Electric Reliability Corporation (NERC) [8] have also reported a reduction in frequency response due to the increasing penetration of RERs. Among the various solutions available for alleviating the aforementioned concerns, the concept of virtual inertia has been widely proposed in the literature [9–11]. Virtual inertia can be defined as the controlled contribution of electrical torque from a unit that is proportional to the RoCoF at the terminals of the unit [12] and can be implemented using ESSs, RERs, power electronic devices, and control algorithms [13]. For example, [14] proposes a control algorithm to minimize frequency disturbances in the system due to reduced inertia using ESS, while [15] discusses the different ways by which power electronic converters can be controlled to behave like virtual synchronous machines. Since many ESS are fast-acting devices with high ramping capabilities, they are well-suited for providing virtual inertia to the system. For this purpose, ESSs need to be sized accurately, depending on the system requirements. The problem of ESS sizing for virtual inertia support has been explored in [16–19]. In [16], the authors have presented a method to estimate the size of ESS to enhance the inertial response of a power system in the presence of high wind penetration level although the loss of system inertia due to component failures were not considered. Probabilistic methods for sizing ESS under high RER penetration considering the loss of inertia due to component failures have been studied in [17, 18] and a techno-economic framework for sizing of ESS is proposed in [19]. However, all prior works have used simulation techniques that can be computationally expensive.

Besides having low inertia characteristics, RERs are also variable in nature. The negative effects of wind variability on the reliability and stability of a power system have been widely reported in the literature [5, 20–22]. These disadvantages of wind power arising due to its variability can be mitigated by several methods, including deployment of ESS, aggregation of geographically diverse wind energy, and the use of flexible loads. The benefits of utilizing ESS for mitigating variability of wind generation have been observed by researchers in the past [23–29]. Of these, [23] was possibly the first to explicitly address reliability benefits. Hu *et al.* in [25] explicitly showed how the installation of ESS mitigates the variability of wind power and improves system reliability by performing reliability evaluation of a wind integrated system. Mitra [27] developed a probabilistic method for determining the size of an ESS to achieve a pre-specified reliability target and then utilized this methodology for quantifying storage required for mitigating the variability of wind power in [28]. Nguyen *et al.* [29] proposed a strategy for improving the reliability of a wind integrated system using ESS under a frequency security constraint. However, although ESS projects are easier and faster to build than new transmission infrastructure, they incur high annual maintenance costs and the battery packs also need to be regularly changed when they reach their end of life. Apart from deploying ESS, the variability of wind energy can also be reduced by aggregating geographically diverse wind farms. Several reports [30–32] have presented evidence that aggregating power outputs of wind farms spread across geographically diverse areas can significantly reduce its variability. Aggregation reduces variability as it leads to an increased tendency of wind power output to lie near its mean value and a decreased tendency for it to lie near its extremes [33]. Another study [34] has concluded that aggregation can even make wind power suitable for serving a percentage of the base load and help in reducing the long-distance transmission capacity of the power grid. Researchers have shown the mathematical models and methods required for evaluating the reliability benefits of wind aggregation using mean variance optimization in [35, 36]. However, several factors can limit the advantages gained by aggregating wind power. In [33], the authors suggest that the degree of smoothing depends on the number of plants and the size of the geographical area over which they are spread, and [37] shows that the smoothing effect decreases with the decrease in the geographical area over which aggregation is considered. Besides, long-term fluctuations in wind speed, e.g., several hours or longer, tend to have higher correlation [38, 39], thus limiting the benefits of aggregation.

While ESSs can be used to alleviate the stability and reliability of the power grid, it is important to note that ESS projects are significantly expensive. Therefore, investment planning frameworks need to be devised for extracting maximum economic benefits from these projects which will aid in attracting more investors and utilities. ESSs traditionally participate in different electricity markets like energy and ancillary markets to generate revenue. In many countries, the power industry has gradually shifted from a centralized operation system to deregulated competitive markets in recent times [40]. In the United States, both regulated and deregulated systems exist today. For some wholesale markets, investor-owned electric utilities own generation facilities as well as transmission and distribution systems and are responsible for operating, managing, and providing power to retail consumers. In other regions, wholesale markets are operated by regional transmission organizations (RTOs) or Independent System Operators (ISOs). These ISOs and RTOs provide buyers and sellers the opportunity to bid for or offer generation for energy and ancillary services in their markets [41]. Some of the biggest electricity markets in the U.S. are operated by the Pennsylvania New Jersey Maryland (PJM) Interconnection, Midcontinent Independent System Operator (MISO), Electricity Reliability Council of Texas (ERCOT), California Independent System Operator (CAISO), and New York Independent System Operator (NYISO). ESSs can participate in several applications in these markets for generating revenue. A variety of applications of ESS have received widespread attention from researchers in the past. Byrne *et al.* [42] presents a summary of the leading applications of grid-connected storage systems. Among the applications of ESS prevalent today, energy arbitrage and frequency regulation have proved to be the most profitable ones according to multiple studies [43–45]. Reference [43] discusses the economic case for ESS in NYISO for the two previously mentioned applications. Authors of [44] present a method for determining the stacked benefits from ESS following the PJM market model while authors in [45] present an approach for maximizing economic benefits from ESS in the MISO electricity market. Although these studies focus on maximizing the economic benefits of ESS, none of these works provide a detailed cost-benefit analysis or considers the degradation of batteries. Hence, a comprehensive investment planning methodology that focuses on the maximum economic benefits of ESS and provides a detailed cost-benefit analysis useful to the investors still needs to be developed.

1.2 Thesis Contributions

This thesis investigates the role of ESSs in alleviating the stability and reliability issues faced by the power grid due to increased RER penetration and develops models and techno-economic optimization frameworks for providing solutions to these problems. The contributions of this thesis can be summarized as follows.

- Developing an analytical approach for sizing of ESSs for grid inertial support
- Developing a method for calculating the probability of synchronization of generating resources in a power system
- Establishing a relationship between the probability of synchronization of a wind farm with its capacity value
- Developing an investment planning framework for ESSs participating in electricity markets
- Modeling the degradation cost of lithium-ion batteries participating in electricity markets
- Developing a techno-economic planning framework for ESSs providing grid inertial support
- Developing a cost-effective transmission planning framework for improving the reliability of wind-rich power systems

1.3 Thesis Organization

The rest of this thesis is organized as follows. Chapter 2 presents an analytical approach for sizing ESSs to provide inertial support to the grid and maintain frequency stability in presence of RERs. Chapter 3 presents a comprehensive investment planning framework for an ESS, which estimates the maximum revenue that the ESS can generate over its lifetime, and provides the necessary tools to investors for aiding the decision-making process regarding ESS projects. A degradation cost model for lithium-ion ESSs is also developed here. In Chapter 4, a techno-economic planning framework is presented which optimally sizes ESSs to alleviate frequency stability issues of wind integrated systems, while minimizing the operational costs by participating in electricity markets. A bi-level stochastic optimization framework is developed here that minimizes the daily operating cost of the grid while satisfying a frequency stability constraint. Chapter 5 presents a cost-effective transmission planning approach for reducing the variability of wind power and enhancing the reliability of a wind-integrated system, by jointly deploying ESS and wind power aggregation. Chapter 6 summarizes the contributions of this thesis and discusses possible future work.

CHAPTER 2

SIZING OF ENERGY STORAGE FOR GRID INERTIAL SUPPORT IN PRESENCE OF RENEWABLE ENERGY

2.1 Introduction

Frequency response plays a vital role in overall power system dynamic performance. An imbalance between the generated power and load power leads to frequency deviation from the nominal values and might result in some undesired conditions including high RoCoF, underfrequency load shedding, higher frequency nadirs, and cascaded outages in some severe cases. In the event of such an imbalance, the rotational kinetic energy stored in the rotor of the conventional synchronous generators is used to provide inertial support to the grid, thus restoring frequency stability. However, RERs like wind or solar are interfaced with the grid through power electronic devices like inverters, thus limiting their capabilities of providing inertial support [3, 4]. On the other hand, since ESSs are fast-acting devices with high ramping capabilities, they are well-suited for providing virtual inertia to the system. For this purpose, ESSs need to be sized accurately, depending on the system requirements. The problem of ESS sizing for virtual inertia support has been explored in [16–19]. In [16], the authors have presented a method to estimate the size of ESS to enhance the inertial response of a power system in the presence of high wind penetration level although the loss of system inertia due to component failures were not considered. Probabilistic methods for sizing ESS under high RER penetration considering the loss of inertia due to component failures have been studied in [17, 18] and a techno-economic framework for sizing of ESS is proposed in [19]. However, all the aforementioned works have used simulation techniques that can be computationally expensive.

In this chapter, we present an *analytical* method that solves the problem of reduced system inertia due to increased RER penetration. Compared to traditional approaches that are based on simulation, analytical methods afford several benefits. Apart from being computationally less demanding, analytical approaches offer a solid mathematical foundation, based on which more complex problems can be solved. Besides, analytical models allow a more intuitive understanding of the problem and often provide the flexibility of performing back-of-the-envelope calculations as the intricacies of the problem evolve. For example, the approach presented here can be used as a foundation for solving more complicated problems such as optimal planning or economic dispatch while maintaining the frequency stability of the grid with the aid of an ESS. Even if simulation becomes necessary for these more complex problems, the utilization of the analytical model can help reduce both the complexity and the computational burden. To demonstrate the efficacy of this analytical approach, we have used simulation techniques to validate the results obtained from the proposed analytical method.

The proposed analytical approach is based on estimating the expected inertia of the generating resources of the system, including conventional generators and RERs. The amount of inertia present in any system constantly varies due to generator outages and the replacement of conventional units with RERs. As the system inertia fluctuates due to the aforementioned reasons, there might be instances when the system will not possess adequate inertia to maintain frequency stability after a disturbance occurs and before the primary frequency response is activated. In such situations, ESSs can provide virtual inertia to the system at a fast rate and maintain frequency stability. For this purpose, ESSs need to be sized accurately, so that they can compensate for the lost inertia.

Considering the loss of inertia due to the two most common issues, generator outages, and RER penetration, we propose an analytical approach that is capable of estimating the size of ESS required to provide inertial support to the grid. This proposed approach involves the construction of a probability distribution of the system inertia, from which its expected value is calculated. While calculating the probability distribution of system inertia, we have also developed a methodology to calculate the probability of synchronization of the generating resources of the system, since the availability of a unit for supporting load does not guarantee that it is synchronized with the system, and this is another major contribution of this work. We have used wind farms as illustrative examples of RERs in this work, but the proposed methodology can be extended to solar as well. Wind farms are modeled as multi-state units and the variability in wind power output due to both variation in wind speed and forced outages of wind turbines are considered.

The contributions of this work can be summarized as follows.

1. For the first time, a *analytical* approach is developed for sizing of ESS to provide inertial support. This analytical approach potentially paves the way for solving more complicated problems related to the frequency stability of the grid with less computational burden and complexity.

2. This proposed analytical approach brings together in its framework the two most common causes of reduced inertia in the system: generator outages and replacement of conventional synchronous generators with RERs.

3. A new method is also developed within the proposed framework to calculate the probability of synchronization of the generating resources of the power system, which is necessary to estimate the probability distribution of system inertia.

The rest of this chapter is organized as follows. The methodology proposed for determining the probability distribution of the system inertia is described in Section 2.2. The modeling of wind farms as multi-state units is discussed in Section 2.3. A maximum frequency deviation limit derived from a generalized LFC model is presented in Section 2.4. Section 2.5 demonstrates some case studies and results while section 2.6 provides some concluding remarks.

2.2 Probability Distribution of System Inertia

The expected inertia of the generating resources can be used as a reference point for estimating the size of ESS required to maintain the frequency stability of the system. The total inertia of the system varies with time due to the outage of generators and the replacement of conventional units with RERs. Hence, to calculate the expected inertia, it is necessary to first construct the probability distribution of the equivalent inertia present in the system. In this work, the conventional units are modeled as two-state units by using their forced outage rates (FORs), while RERs illustrated by wind farms are modeled as multi-state units for determining the probabilities of their outage states.

It should, however, be noted that knowledge regarding the availability of generators is not sufficient for determining the probability distribution of system inertia. This is because the availability of a generator for supporting load does not guarantee that it is synchronized with the system. It simply means that it is available for synchronization when called upon. However, a generator must already be synchronized with the system in order to provide inertial support when there is an imbalance between demand and generation.

2.2.1 Probability of Synchronization

The probability of synchronization of the units can be determined by first calculating the expected energy produced by a unit for a given time horizon, and then taking the ratio of this expected energy and the total energy capacity of the unit for the same time horizon. Therefore, the probability of unit i being committed, p_{ci}, can be expressed as follows.

$$p_{ci} = \frac{E_i^G}{G_i \times T} \tag{2.1}$$

where G_i is the generation capacity of unit i, and the expected energy produced by the unit for a time period T is E_i^G.

The expected energy produced by a unit can be calculated by using a production cost model as proposed in [46]. First, the equivalent load of the system, which comprises both the actual load and the capacity on outage, is expressed in terms of a random number L_e as follows.

$$L_e = L + X \tag{2.2}$$

where L and X are random numbers representing the total system load and the total generation capacity on outage, respectively. The probability distribution of the equivalent load, $P(L_e)$, can be obtained by the convolution of the probability distributions of the components of L_e.

The probability distribution for the system load, L, can be derived by scanning the hourly load data of the system over the period of interest, while the probability distribution for the capacity on outage, X, can be derived as a capacity outage probability table (COPT) [47]. In general, when adding a new two-state unit (with states *up* and *down*) of capacity C, forced outage rate q, the cumulative probability of an outage state X can be determined by the following expression.

$$P(X) = \bar{P}(X)(1-q) + \bar{P}(X-C)q \tag{2.3}$$

where $\bar{P}(X)$ is the cumulative probability of outage state X before the addition of the new unit. In case of multi-state units, like wind farms, (2.3) should be modified as follows.

$$P(X) = \sum_{i=1}^{n} p_i \times \bar{P}(X - C_i) \tag{2.4}$$

where p_i is the probability of state i of a unit with n states.

Next, in order to determine the expected energy of the generator units, it is necessary to successively deconvolve the probability distribution of each unit from the distribution of the equivalent load [48, 49]. This can be accomplished by rewriting (2.3) as a deconvolution formula as follows.

$$\bar{P}(X) = \frac{P(X) - q\bar{P}(X-C)}{(1-q)} \tag{2.5}$$

One advantage of this method is that the addition or removal of units from the distributions may be obtained by operating directly on the convolved distribution of $P(L_e)$, which leads to a significant reduction of computation times [46].

This deconvolution process is implemented in this study as follows. Let there be N generating units in the system, the total installed capacity be G_N and let the probability distribution of the equivalent load be defined as $P_N(L_e)$ when all units are considered. Now, let us consider that the unit with the highest generating cost is removed from the system. The installed capacity is reduced to G_{N-1} and the corresponding probability distribution of the equivalent load becomes $P_{N-1}(L_e)$. The expected value of the energy generated by the removed plant, E_N^G, can then be expressed as follows [46].

$$E_N^G = T \int_{P_{N-1}}^{P_N} p_N P_{N-1}(L_e) d(L_e) \tag{2.6}$$

where p_N denotes the availability of the removed generator and T is the period of interest. Thus, by successively removing generator units in decreasing order of their generating costs, the expected energy produced by all the units in the system can be determined. This information can then be combined with (2.1) to determine the probability of each unit being committed.

2.2.2 Expectation of System Inertia

The probability distribution, and hence the expected value of the system inertia can now be determined from the probability of commitment of each unit as derived in the previous section. Let H be a random variable representing the system inertia. It should be noted that H is a discrete random variable since it only assumes values that are equal to the sum of inertia constants of some or all units. Let U be the set of generators synchronized with the system and D be the set of generators not synchronized to the system. The probability mass function of the random variable H can be then represented as follows.

$$P\{H = h\} = \prod_{\substack{i \in U \\ j \in D}} p_{ci} q_{cj} \tag{2.7}$$

where p_{ci} is the probability of commitment of the i^{th} generator, $q_{ci} = 1 - p_{ci}$, and h is expressed as follows.

$$h = \frac{\sum_{i \in U} H_i S_i}{S_{\text{eq}}} \tag{2.8}$$

Then, the expectation of H can be calculated as:

$$E[H] = \sum_{h \in H} h P\{H = h\} \tag{2.9}$$

This value of $E[H]$ is used to determine the required size of the ESS.

2.2.3 Probability of Synchronization of Wind Farms

Although wind farms are unable to provide any mechanical inertial support due to their connection with the grid via power electronic devices, some amount of virtual inertia might still be extracted by using certain control techniques. However, since wind farms are not generally dispatched in the order of their generating costs like conventional units, the deconvolution method described in section

2.2.1 cannot be employed to calculate the probability of synchronization of wind farms. Instead, the capacity value of wind farms can be used for calculating their probability of synchronization. In this context, consider the following postulate.

Postulate: The probability of synchronization of a wind farm (p_{cw}) is equal to its capacity value (CV_w), or,

$$p_{cw} = CV_w \tag{2.10}$$

Proof: Capacity value can be defined as the amount of additional load that can be served due to the addition of a unit while maintaining the existing level of reliability [50]. Let P_w be the additional load that can be supported due to the addition of a wind farm of nameplate capacity G_w. If the new wind farm supports this load for T units of time, then the energy absorbed by the load from the wind farm is given as:

$$E_w = P_w \times T \tag{2.11}$$

The CV of the wind farm can then be mathematically expressed as follows.

$$CV_w = \frac{E_w}{G_w \times T} \tag{2.12}$$

Comparing (2.12) with (2.1), we see that just like CV, the probability of synchronization also represents the amount of energy that the system absorbs from a unit for serving load. Thus, it can be concluded that in the context of this work, the probability of synchronization of a wind farm is essentially equal to its CV.

The validity of this equivalence is also supported using Monte Carlo simulation, which makes no assumptions regarding the probability of synchronization and the CV of a wind farm, but still produces results very close to those obtained using the analytical method.

2.3 Modeling of Wind Farms

Wind farms are modeled as multi-state units in this work. The variability in wind power output due to both variation in wind speed and forced outages of turbines are considered.

2.3.1 Modeling of Wind Speed

Wind speed can be approximated by a discrete Markov chain with a finite number of states. The probability, frequency, and transition rate of each wind state can be estimated from a large number of samples of wind speed time-series data. The probability of each wind state is determined as follows [51].

$$p_{c,i} = \frac{\sum_{j=1}^{N} n_{ij}}{\sum_{k=1}^{N} \sum_{j=1}^{N} n_{kj}} \tag{2.13}$$

where $p_{c,i}$ is the probability of wind being in state i, n_{ij} is the number of transitions from state i to state j, and N is the total number of states. These wind speed states can be easily converted to wind power output states by utilizing the power curve of a wind turbine [52].

2.3.2 Modeling of Wind Farm Capacity Outage

Wind farms generally comprise of a number of wind turbines, where the wind turbines can be modeled as two-state units (*up* and *down*) with known failure and repair rates λ and μ respectively, similar to conventional units. Hence, a COPT can be built for a wind farm, say COPT$_w$, considering the forced outage rate of the wind turbines, by using equation (2.3). COPT$_w$ is then combined with the wind power states earlier obtained in section 2.3.1 to construct the multi-state unit of the wind farm, as described in [6]. The multi-state wind farm unit thus developed can then be added to the COPT of the system by using (2.4).

2.4 Frequency Stability of Power Grid

The control of frequency and power generation is commonly referred to as load frequency control (LFC). It consists of the following stages: inertial response, primary frequency response (PFR), secondary frequency response (also known as automatic generation control or AGC), and tertiary frequency response [53]. This work focuses on the inertial response of the grid. The following sections describe how the frequency dynamics are affected by the equivalent inertia of the system and the generalized LFC model used to calculate the minimum inertia required by the system to maintain frequency stability.

2.4.1 Modeling of Grid Frequency Response

Frequency response plays a vital role in overall system dynamic performance. An imbalance in real power leads to frequency deviation from the nominal values and might result in load shedding. One of the most important components of frequency response is the inertia constant of a conventional generator, H, which is defined as follows [54].

$$H = \frac{1}{2}J\omega^2 \tag{2.14}$$

where J is the moment of inertia and ω represents the rotational speed of the rotor. In other words, H is a measure of the amount of kinetic energy stored in the rotor of a synchronous generator. Also, the equivalent inertia constant of a system composed of n generators can be determined as follows [16].

$$H_{\text{eq}} = \frac{\sum_{i=1}^{n} H_i S_i}{S_{\text{eq}}} \tag{2.15}$$

where H_i and S_i are the inertia constant and nominal power of the i^{th} unit and S_{eq} is the total rated power of the system. The swing equation, which describes the motion of a machine, can be expressed as follows [55].

$$\frac{2H_{\text{eq}}}{f_s}\frac{df}{dt} = \frac{P_m - P_e}{S_{\text{eq}}} = \frac{\Delta P}{S_{\text{eq}}} \tag{2.16}$$

where f_s is the nominal frequency of the system, $\frac{df}{dt}$ is the RoCoF, P_m and P_e are the mechanical power input and the electrical power output, respectively.

2.4.2 Load Frequency Control Model

A generalized LFC model is utilized in this study [56], which is capable of representing the contribution of each governor to the system frequency control. The model of LFC for a multi-machine system is illustrated in Fig 2.1 [56]. A summary of the notations used in Fig. 2.1 is given

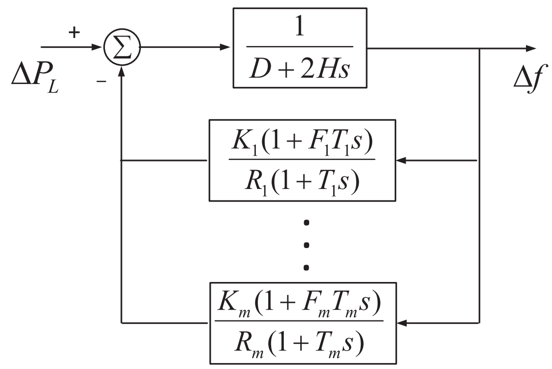

Figure 2.1: LFC model of a multi-machine system.

as follows.

H = equivalent inertia constant;

D = load damping constant;

K_i = LFC controller of machine i;

R_i = equivalent regulation constant of machine i

F_i = fraction of turbine power generated by
high pressure (HP) unit of machine i;

T_i = governor time constant of machine i;

Δf = frequency deviation;

ΔP_L = disturbance

The governor time constants of all machines are assumed to be of equal value since the maximum frequency deviation has a low sensitivity to this quantity (T_R) [56].

2.4.3 Minimum Inertia Required

The minimum inertia required by the system to maintain frequency stability in the event of a disturbance is discussed in this section. The equation for frequency deviation can be developed from the LFC model of multi-machine system [57] and is shown in (2.17).

$$\Delta f(s) = \frac{\frac{\Delta P_L}{s}}{D + 2Hs + \sum_{i=1}^{m} \frac{K_i(1+F_i T_R s)}{R_i(1+T_R s)}} \tag{2.17}$$

Assuming all values of T_R to be identical and using inverse Laplace transformation, the expression for frequency deviation in the time domain is obtained as follows.

$$\begin{aligned}\Delta f(t) = \frac{\Delta P_L}{2HT_R\omega_n^2}\Bigg(1 - \frac{1}{\sqrt{1-\zeta^2}} e^{-\zeta\omega_n t} \cos\,(\omega_n\sqrt{1-\zeta^2}t \\ - \phi)\Bigg) + \frac{\Delta P_L}{2H\omega_n\sqrt{1-\zeta^2}} e^{-\zeta\omega_n t} \sin\,(\omega_n\sqrt{1-\zeta^2}t)\Bigg)\end{aligned} \tag{2.18}$$

where

$$F_R = \sum_{i=1}^{m} \frac{K_i F_i}{R_i} \tag{2.19}$$

$$R_R = \sum_{i=1}^{m} \frac{K_i}{R_i} \tag{2.20}$$

$$\omega_n = \sqrt{\frac{1}{2HT_R}(D + R_R)} \tag{2.21}$$

$$\zeta = \frac{1}{2}\frac{2H + T_R(D + F_R)}{\sqrt{2HT_R(D + R_R)}} \tag{2.22}$$

$$\phi = \tan^{-1}\left(\frac{\zeta}{\sqrt{1-\zeta^2}}\right) \tag{2.23}$$

The maximum frequency deviation is obtained by equating the derivative of $\Delta f(t)$ in (2.18) to zero and is expressed as follows.

$$\Delta f_{\max} = \frac{\Delta P_L}{R_R + D}\left(1 + e^{-\zeta\omega_n t_{\max}}\sqrt{\frac{T_R(R_R - F_R)}{2H}}\right) \tag{2.24}$$

where

$$t_{\max} = \frac{1}{\omega_n\sqrt{1-\zeta^2}} \tan^{-1}\left(\frac{\omega_n\sqrt{1-\zeta^2}}{\zeta\omega_n - 1/T_R}\right) \tag{2.25}$$

2.4.4 Minimum Inertia Required in a Wind-Integrated System

The total inertia of the system is reduced when conventional generators with high rotating masses are replaced by wind generators with low inertia. This reduction of inertia is modeled into the maximum frequency deviation limit as follows [58]. It is assumed that the reduction in the system inertia due to the removal of a conventional unit is γ_{cv} and the contribution from the wind turbines is γ_w. Then, the new values of system inertia and the equivalent regulation constant can be expressed as follows.

$$H_{\text{new}} = H_{\text{old}}(1 - \gamma_{cv} + \gamma_w) = \gamma H_{\text{old}} \tag{2.26}$$

$$R_{\text{new}} = \frac{R_{\text{old}}}{(1 - \gamma_{cv} + \gamma_w)} = \frac{R_{\text{old}}}{\gamma} \tag{2.27}$$

The changes in the values for the system inertia and the regulation constant leads to the following modification in the expression for the maximum frequency deviation.

$$\Delta f_{\max}^{\text{new}} = \frac{\Delta P_L}{\gamma R_{\text{Rnew}} + D}\left(1 + e^{-\zeta_{\text{new}}\omega_{n,\text{new}}t_{\max}^{\text{new}}}\sqrt{\frac{T_R(R_{\text{Rnew}} - F_{\text{Rnew}})}{2H_{\text{new}}}}\right) \tag{2.28}$$

where

$$F_{\text{Rnew}} = \sum_{i=1}^{m} \gamma \frac{K_i F_i}{R_i} = \gamma F_R \tag{2.29}$$

$$R_{\text{Rnew}} = \sum_{i=1}^{m} \gamma \frac{K_i}{R_i} = \gamma R_R \tag{2.30}$$

$$\omega_{n,\text{new}} = \sqrt{\frac{1}{2H_{\text{new}}T_R}(D + R_{\text{Rnew}})} \tag{2.31}$$

$$\zeta_{\text{new}} = \frac{1}{2}\frac{2H_{\text{new}} + T_R(D + F_{\text{Rnew}})}{\sqrt{2H_{\text{new}}T_R(D + R_{\text{Rnew}})}} \tag{2.32}$$

The minimum inertia required to maintain frequency stability can now be determined from (2.24) for a system with only conventional generation and (2.28) for a wind-integrated system by using a pre-determined value for $\Delta f_{\max}$. For example, for a system operating with a nominal frequency of 60 Hz, $\Delta f_{\max}$ can be set at 0.1 Hz. The above model can be used to simulate system response for load disturbances as well as generator or other equipment failures.

2.4.5 Contribution of ESS towards Frequency Stability

Let the minimum inertia level that is required to maintain frequency stability be H_{min} for a particular disturbance event. Also, let the equivalent inertia of a system be $H_{\mathrm{sys}}(t)$ at any time t. If $H_{\mathrm{sys}}(t) < H_{\mathrm{min}}$, then an ESS may be deployed, which can inject active power into the system at a sufficiently high rate to maintain frequency stability. Hence, the inertia that the ESS needs to provide for a particular disturbance at any time t, if $H_{\mathrm{sys}}(t) < H_{\mathrm{min}}$, can be defined as follows.

$$H_{\mathrm{ESS}}(t) = H_{\mathrm{min}} - H_{\mathrm{sys}}(t) \tag{2.33}$$

The ESS is sized based on the expected value of the system inertia, $E[H_{\mathrm{ESS}}(t)]$ or H_{ESS}, which is calculated as follows.

$$H_{\mathrm{ESS}} = H_{\mathrm{min}} - E[H_{\mathrm{sys}}(t)] \tag{2.34}$$

where H_{min} is constant for a particular disturbance event and $E[H_{\mathrm{sys}}(t)]$ is determined by the method proposed in section 2.2.2.

Now, the relationship between H_{ESS}, and the real power required to be injected by the ESS for maintaining frequency stability, P_{ESS}, can be derived from (2.16) as follows [16].

$$H_{\mathrm{ESS}} = P_{\mathrm{ESS}} \frac{f_s}{2} \left(\frac{df}{dt} \right)^{-1} \tag{2.35}$$

In (2.35), the expression $\frac{df}{dt}$ or the RoCoF can be defined as a measure of how quickly the frequency changes following a sudden imbalance between generation and load [59] and is most commonly expressed in Hz per second. The initial RoCoF is calculated as the change in frequency over a 0.5 second period immediately following a sudden generation loss [60]. The initial RoCoF depends on several factors including the magnitude of the disturbance event, the amount of system inertia online, and the speed and magnitude of the frequency response. If the initial RoCoF is significantly high, then the system frequency may fall at a level where underfrequency load shedding (UFLS) may be required, the UFLS requirements for the North American grid being provided in [61]. Therefore, the RoCoF should be restricted within a certain value to avoid UFLS. According to [16], the value of RoCoF should not exceed 0.5 Hz/s. In this work, the value of RoCoF is assumed to be a constant value of 0.5 Hz/s, thus considering the worst-case scenario.

2.5 Case Studies and Results

Data from the New England IEEE 39-bus system [62] is used to test the efficacy of the proposed method. The original test system comprises 39 buses, 10 generators, and 46 transmission lines. A single line diagram of this test system and all relevant system data are shown in Appendix A. Part of the conventional generation is replaced by wind farms in some of the case studies presented in this work, to illustrate the effect of RER integration on system inertia. Wind speed data from [63] is used to model wind farms as multi-state units, as described in section 2.3. The CV of the wind farm is calculated in terms of the probability of synchronization to be 0.15 for the data-set used in this work. The annual hourly load curve is obtained from [64] and adjusted according to the peak load of the test system. Data for the governor parameters are obtained from [56] and reliability data for the generating units are obtained from [65].

2.5.1 Probability of Synchronization

The probability distribution of the equivalent load of the system, L_e, is illustrated in Fig. 2.2, which also shows how the distribution of the equivalent load changes as units are gradually removed from the system using deconvolution. When all units have been removed, the distribution of the equivalent load coincides with the load duration curve. The probability of synchronization for each unit is calculated using the method described in section 2.2, and the results are shown in Table 2.1. These results can be utilized to determine the probability distribution of system inertia and its expected value. The probability distribution of the system inertia is shown in Fig. 2.3. The random variable representing the system inertia, H, ranges from 0 to 792.7 s, and the expected value of the system inertia, $E[H]$ is calculated to be 581.62 s for the original test system without any wind power penetration.

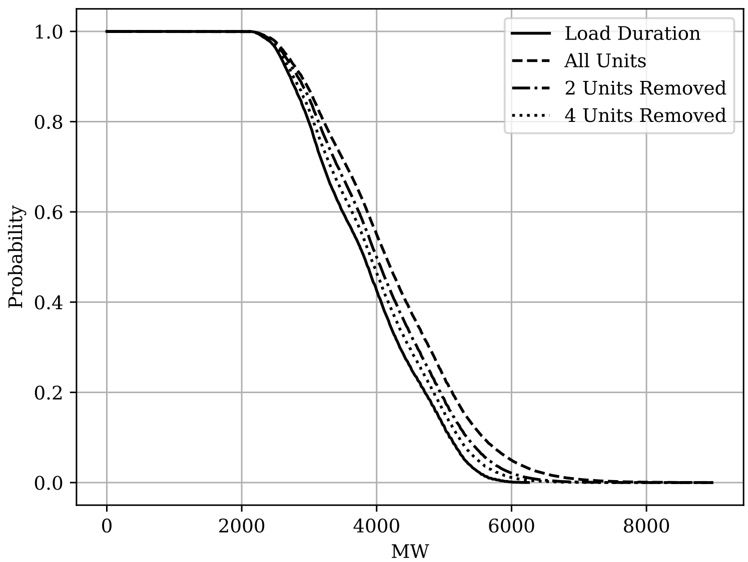

Figure 2.2: Probability distribution of equivalent load and the load duration curve for the IEEE 39 bus system.

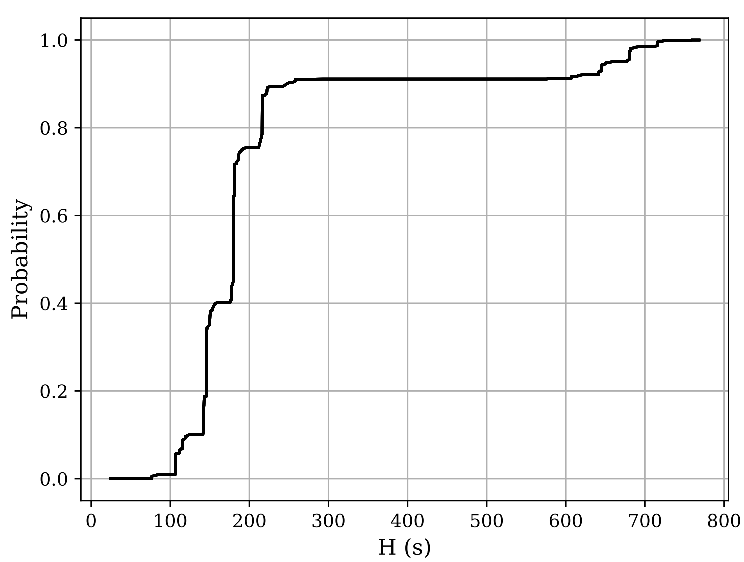

Figure 2.3: Cumulative Distribution Function of H.

Table 2.1: Expected energy output for one year.

Unit No.	Expected Energy per year (MWh)	p_c
1	8,298,663	0.911
2	602,674	0.106
3	4,394,496	0.692
4	1,365,113	0.239
5	19,889	0.005
6	2,744,060	0.456
7	170,530	0.034
8	69,397	0.014
9	7,014,167	0.926
10	9,102,311	0.945

2.5.2 Case Studies

The ESS sizing approach proposed in this work is illustrated with the help of three cases, by varying the degree of wind penetration in each case. Disturbance in the form of a load of 0.1 p.u. is assumed to change the system frequency from its nominal value of 60 Hz. ESS sizes for three values of maximum frequency deviation (Δf_{max}) are determined for each case. In general, the proposed approach can be used to size ESS devices for any value of maximum frequency deviation and any load disturbance. This provides the system operator with ample flexibility in choosing the parameters. Data for the inertia constant of wind farms are obtained from [58].

1. **Case 1:** The original system with only conventional generation is considered in this case.

2. **Case 2:** About 8% of the generation capacity of the system (the current share of installed wind capacity in the U.S. today) is replaced by wind generation. To achieve this, a conventional unit of 580 MW is removed from the system and replaced by a wind farm of capacity 640 MW. This wind farm is assumed to consist of 80 identical wind turbines, of 8 MW each.

3. **Case 3:** About 20% of the generation capacity of the system (target wind power share in the U.S by 2030 [30]) is replaced by a wind farm of capacity 1520 MW. Two conventional units with capacities of 646 MW and 865 MW are removed to achieve this.

2.5.3 Frequency Deviation Limit

The minimum inertia required to maintain the frequency deviation of the system within pre-specified limits under a load disturbance is determined here from (2.24) for a system with only conventional generation and (2.28) for wind-integrated systems. Fig. 2.4 illustrates how the maximum frequency deviation of the system increases with decreasing system inertia for a load disturbance of 0.1 p.u. In this work, the size of the ESS is determined based on the difference between the expected

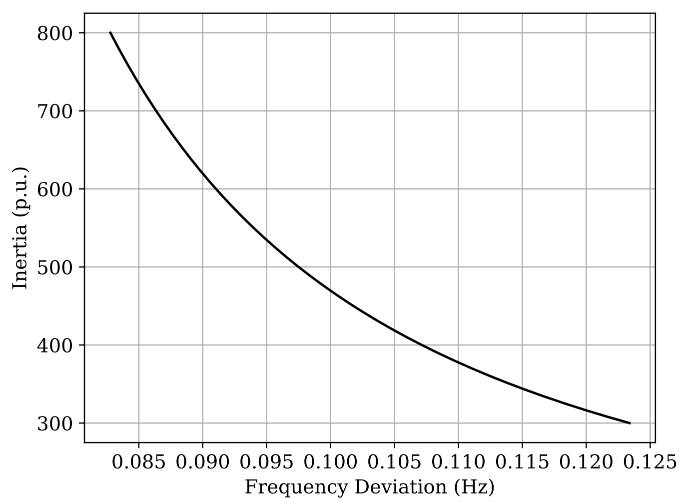

Figure 2.4: Maximum frequency deviation vs. inertia for the IEEE 39 bus system for a load disturbance of 0.1 p.u.

value of the system equivalent inertia and the minimum inertia required to maintain frequency stability. However, since the proposed approach involves the construction of the entire probability distribution of system inertia, other statistics besides the mean value can be easily extracted from the distribution. This provides the system planner with the flexibility to evaluate the risk of losing frequency stability associated with installing different sizes of ESS.

2.5.4 ESS Size

Results for the three cases are shown in Table 2.2. The energy capacity of the ESS would depend upon several factors, including how frequently it is called upon by the RTO to provide synthetic inertia, the system behavior, and also the charge-discharge characteristics of the ESS. If the ESS facility is designed to provide other services in addition to synthetic inertia, these services will also be considered in determining the energy capacity. Although the location of the ESS is not explicitly determined in this work, given that it is the wind farm that displaces system inertia, the ESS should be located near the wind farm for providing virtual inertia support. In case there are multiple RERs, the total ESS capacity required can be distributed proportionately among all locations containing the RERs.

Table 2.2: ESS sizes for a load disturbance of 0.1 p.u.

Case	Freq. Dev. Limit (Hz)	**E[H]** (s)	$\mathbf{H_{min}}$ (s)	$\mathbf{H_{ESS}}$ (s)	$\mathbf{P_{ESS}}$ (MW)
1	0.085		734	152	253
	0.09	582	619	39	62
	0.095		531	N/A	N/A
2	0.085		787	219	365
	0.09	568	659	91	152
	0.095		557	N/A	N/A
3	0.085		875	315	525
	0.09	560	728	168	280
	0.095		608	48	80

Results show that for the first two cases, an ESS is only required when the maximum frequency deviation of the system has to be restricted to 0.09 Hz. The system in both cases possesses adequate inertia to limit the frequency deviation beyond 0.09 Hz. For Case 3, however, since the wind penetration is significantly higher than Case 2, an ESS is required to limit the maximum frequency deviation up to 0.095 Hz. This also implies that as the penetration of RERs keeps on increasing, larger ESSs will be required in the future for restricting system frequency deviations. Results obtained by employing the analytical approach are then validated using Monte Carlo simulation (MCS). Using MCS, the mean inertia of the system for cases 1, 2, and 3 are calculated to be 595 s, 587 s, and 569 s, respectively. Comparing these results with those presented in Table 2.2, we can see that the mean inertia obtained by both methodologies lies within approximately 3% of each other for each case. This validation proves the efficacy of the proposed analytical approach and emphasizes its utility in sizing of ESS for grid frequency stability without having to bear the high computational burden of simulation methodologies.

2.5.5 Effect of Incorporating Transmission Constraints

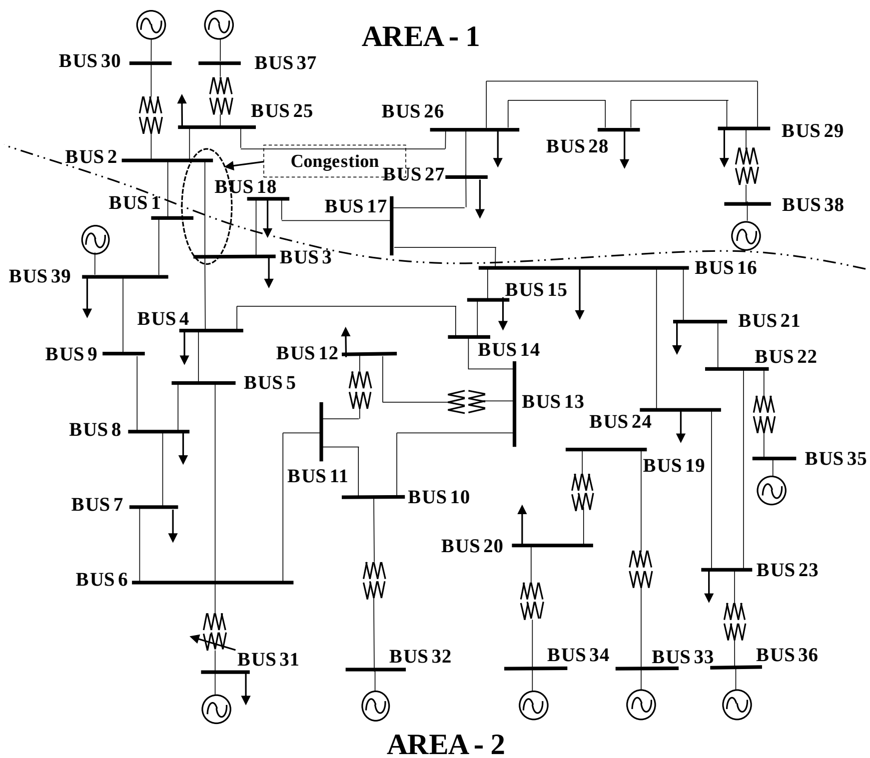

Figure 2.5: A single line diagram of the IEEE 39 bus system illustrating the multi-area system and congestion.

The results of the proposed analytical approach in estimating the system inertia are compared with the results of a simulation technique that considers the transmission constraints of the system. Case 2 is used for the purpose of this comparison. For this case, the mean inertia of the system considering the transmission constraints is calculated to be 639 s, which is significantly higher than 568 s, the result obtained using the analytical method. The reason for this mismatch is investigated and a congestion is identified in the transmission line between buses 2 and 3. The system is then split into two equivalent areas, as shown in Fig. 2.5, to avoid this congestion. The expected inertia values for areas 1 and 2 are then calculated using the analytical approach to be 528 s and 96 s, respectively. The expected inertia values of the individual areas add up to 624 s, which is within 2% of the value obtained using MCS. This shows that the proposed analytical approach is valid for multi-area systems even when the transmission constraints are considered. Also, system operators typically have knowledge regarding the areas of congestion in the system. Therefore, they can use the proposed analytical method to perform back-of-the-envelope calculations to allocate the necessary amounts of storage required by each zone to provide inertial support. This further emphasizes the efficacy of the proposed approach, since a practical power system generally comprises multiple areas controlled by different balancing authorities.

2.6 Conclusion

This chapter presents a novel analytical method for sizing of ESS for providing grid inertial support in presence of RERs. The proposed approach is based on estimating the expected inertia of the system, consisting of conventional generators and RERs. It involves the construction of the probability distribution of system inertia, taking into account generator outages and the replacement of conventional units with RERs. The reduction of system inertia due to various degrees of RER penetration and the sizes of ESS required are calculated and illustrated using a few case studies. The results obtained using the proposed analytical approach are validated using Monte Carlo simulation and the efficacy of this approach is demonstrated for multi-area systems when transmission constraints are considered. This approach also offers system planners flexibility regarding the choice of certain system parameters and the option of risk assessment for different ESS sizes. Future work involves the integration of this approach into an optimal ESS planning framework, that would also allow the economic assessment of ensuring frequency stability of the grid using ESS.

CHAPTER 3

TECHNO-ECONOMIC EVALUATION OF ENERGY STORAGE SYSTEMS

3.1 Introduction

Increasing uncertainty in the modern power grid due to the variability of RERs has led to the widespread deployment of ESSs. ESSs are flexible devices with high ramp rates that can help in maintaining a balance between generation and demand in the face of such uncertainty. ESSs can be deployed for various applications including frequency regulation, peak shaving, voltage support, energy arbitrage, and firming up of RERs. While a few of the applications are capable of generating direct monetary benefits, most are not. However, ESS projects are significantly expensive. Therefore, investment planning frameworks need to be devised for extracting maximum economic benefits from these projects which will aid in attracting more investors and utilities.

ESSs can participate in a number of applications in these markets for generating revenue. A variety of applications of ESS have received widespread attention from researchers in the past. Byrne *et al.* [42] presents a summary of the leading applications of grid-connected storage systems. Among the applications of ESSs prevalent today, energy arbitrage and frequency regulation have proved to be the most profitable ones according to multiple studies [43–45]. Reference [43] discusses the economic case for ESSs in NYISO for the two previously mentioned applications. Authors of [44] present a method for determining the stacked benefits from ESSs following the PJM market model while authors in [45] present an approach for maximizing economic benefits from ESSs in the MISO electricity market. Although these studies focus on maximizing the economic benefits of ESSs, none of them provides a detailed cost-benefit analysis or takes the degradation of batteries into consideration. On the other hand, [66–68] present various strategies

The content of this chapter has been reproduced with permission from *Atri Bera, Saleh Almasabi, Yuting Tian, Raymond H. Byrne, Babu Chalamala, Tu A. Nguyen, and Joydeep Mitra. "Maximising the investment returns of a grid-connected battery considering degradation cost," IET Generation, Transmission & Distribution, vol. 14, no. 21 (2020), pp. 4711 – 4718.*

for co-optimization of ESSs for participating in multiple services. However, a comprehensive investment planning methodology that focuses on the maximum economic benefits of ESSs and provides a detailed cost-benefit analysis useful to the investors still needs to be developed.

Several technologies exist today for grid-level ESSs. The most popular among these are batteries, pumped-hydro storage (PHS), flywheels, and capacitors [69, 70]. The deployment of batteries has increased significantly in the U.S in recent years, with installation capacities growing almost two-folds annually since 2011 [71]. By the end of 2017, the installed battery capacity in PJM was 287.5 MW, and the total installed battery capacity in the U.S. was 708 MW [72]. Among different grid-level battery technologies, lithium-ion batteries are the most popular, constituting more than 80% of large-scale battery storage in operation in the U.S. by the end of 2016 [71]. Several characteristics of Li-ion batteries contribute to their popularity: high efficiency, high energy density, and fast response times.

While estimating the revenue generated from a battery energy storage system (BESS), degradation of batteries should be taken into account as it can affect the accuracy of results. Studies have shown that the degradation of batteries is application-specific. Peterson *et al.* [73] discuss the degradation of batteries for vehicle-to-grid applications, references [74–76] discuss various degradation cost models for economical operation of microgrids, while [77] proposes a piece-wise linear cost function to model aging of batteries due to cycling from participation in electricity markets. References [74–76] consider both the cycle life and the energy throughput while modeling the degradation cost of batteries for improved economic operation of microgrids. Although the degradation cost function has been used to minimize the life loss of the battery in [74–76], the cost of the battery packs was not considered. On the other hand, in [77], the authors consider the cost of the battery but not the lifetime energy throughput. The model proposed in [77] penalizes the battery for every cycle of its operation and this requires the counting of cycles online. However, in practice, cycle counts are tracked using the Rainflow Counting Algorithm (RCA) [78] which requires the entire time-series operation data of the battery and hence cannot be implemented online. As a result, the model proposed in [77] relies on certain approximations that can lead to inaccurate results. Hence, a degradation cost model considering both cycle life and energy throughput, along with the cost of batteries needs to be developed for ESSs participating in electricity markets. This degradation cost model would enable the representation of the degradation cost in monetary units, thus providing the investors with a more realistic estimate of the ROI and payback period.

In recent times, the prices of Li-ion batteries have decreased significantly. While the price of these batteries in 2010 was more than $1000/kWh, in 2020 it has decreased to around $200/kWh [79]. However, utilities are still struggling to make BESS projects profitable due to high capital and daily operating costs. Also, there are only a handful of applications in the electricity markets that reward the storage units monetarily, e.g., energy arbitrage, frequency regulation, spinning reserve, and black start among others. In such a scenario, new methodologies need to be developed for extracting the maximum economic benefits for BESS projects. This work presents a new approach by developing a comprehensive planning framework that enables the BESS to maximize economic benefits while also incorporating the degradation cost of batteries. The lifetime revenue of the BESS is calculated considering battery degradation and a cost-benefit analysis is also performed to provide investors with appropriate tools for making decisions. The applications of the BESS selected for this study are energy arbitrage and frequency regulation. The proposed framework also provides a methodology to determine the optimal location which maximizes the economic benefits. The widespread popularity of Li-ion batteries due to the characteristics mentioned earlier makes it the choice of the BESS for this study. The battery degradation cost is incorporated as a component of the objective function. The degradation cost function in this work is developed specifically for BESS participating in the electricity markets considering both the cycle life and the energy throughput of the battery. Calculating the degradation cost with respect to the energy throughput is advantageous to calculate the cost per cycle since the former can be easily determined for every period while the latter can only be determined after the entire time-series data for the operation of the BESS is available, which may lead to inaccurate results.

The economic benefits from the BESS are maximized by developing an optimization framework. The objective function of this optimization framework includes the revenue from the applications, and the degradation cost of the battery modeled as a penalty function. It also provides the option of optimally locating the BESS when such an opportunity exists. The constraints include the capacity and operational limitations of the BESS and the characteristics of the power system network it is connected to. The proposed optimization framework is linear. Previously, in [80], the authors had proposed a Mixed Integer Non-Linear Programming (MINLP) problem for maximizing the economic benefits of ESSs. However, MINLP problems are computationally complex and the scalability of such problems for big systems might be challenging. Hence, a linear framework is proposed here, which can be scaled irrespective of the system size. The proposed framework estimates the lifetime revenue of a BESS and provides a comprehensive cost-benefit analysis for the BESS project. The revenue is estimated both with and without considering the degradation cost. The results show a significant difference between the two values and underline the importance of considering the degradation cost within the framework. The main contributions of this work can be summarized as follows.

1. This work presents a new framework for a comprehensive investment planning study of grid-connected storage systems with the objective of maximizing economic benefits. This framework is capable of including multiple products (such as energy arbitrage and frequency regulation) as well the battery degradation cost, along with a comprehensive set of operating constraints.

2. This work also adds to the prior art by proposing an improved degradation cost model for Li-ion batteries participating in the electricity markets and incorporating it within the optimization framework as an operational expense. This new degradation cost model considers both the lifetime energy throughput and the cycle count of the batteries. It also considers the cost of the battery packs which reflects the cost of degradation in monetary units. All these aspects have not been considered together in prior literature while modeling the degradation cost of BESSs participating in electricity markets.

3. The framework developed in this work includes the methodology for an exhaustive cost-

benefit analysis of BESS projects that can aid in the decision-making process of investors and utilities in the planning phase based on the net present value, return on investment, and the payback period.

3.2 Participation in the Electricity Market

Only a few applications in the U.S. electricity markets provide economic opportunities for storage systems. These include energy arbitrage, frequency regulation, spinning reserve, and black start among others. A general framework is first developed to quantify the revenue generated by a BESS by participating in any of the market services. For this study, energy arbitrage and frequency regulation are then chosen to demonstrate the efficacy of the proposed framework.

3.2.1 Revenue Model of BESS

A BESS can participate in multiple market services to generate revenue. A general framework is developed in this section to quantify this revenue from any service that the BESS participates in. Let the BESS participate in n market services. Then, the revenue from the i^{th} service, J_i, can be expressed as follows.

$$J_i = f_i(t, q_i(t), m_i(t)) \tag{3.1}$$

where f_i is a function of time t, $q_i(t)$ is the energy exchanged through the BESS and $m_i(t)$ is the value of the market parameters at time t. Hence, the total revenue generated by the BESS from n services, J, for a given time horizon T can be expressed as follows.

$$J = \sum_{t=1}^{T} \sum_{i=1}^{n} f_i(t, q_i(t), m_i(t)) \tag{3.2}$$

Energy arbitrage and frequency regulation are the services selected for this study. However, this framework can be easily extended to include other applications as well.

3.2.2 Energy Arbitrage

Energy arbitrage is one of the oldest and most common applications of storage systems. The revenue from this application depends on the temporal variability in the price of electricity. The price of electricity at a bus in the network is indicated by the locational marginal price (LMP) and depends on the geographic location, variation in load, and connectivity of the bus with the rest of the network. The uncertainties in the load also give rise to uncertainties in the LMPs. For this reason, the LMPs are modeled as random variables in this work. Historical LMP data is used to estimate the distribution of LMPs, and the LMP for each hour is represented by a random variable. The weekly LMP cycle is preserved while fitting the distribution. The random variable representing the LMP for a particular hour is found to be following a normal distribution. The mean and variance of the normal distribution are determined from historical data. The hourly LMPs for the system are generated using the estimated normal distributions.

The BESS takes advantage of the temporal difference in the LMPs to generate profits. It should be noted that the sizes of the BESS considered in this study are significantly smaller than the peak load of the system. Hence, the BESS follows the price taker model, not the price maker model. In other words, the size of the BESS is too small to influence the LMPs of the system [44, 77]. Therefore, J_{arb}, the revenue generated from the energy market, is expressed as follows.

$$J_{\text{arb}} = \sum_{t=1}^{T} \lambda_{\text{lmp}}(t)[q_d(t) - q_r(t)] \tag{3.3}$$

where $\lambda_{\text{lmp}}(t)$ is the LMP at time t, $q_d(t)$ and $q_r(t)$ are the quantities of energy sold to and purchased from the market by the BESS at time t.

3.2.3 Frequency Regulation

The Real Power Balancing Control Performance (BAL001) and Disturbance Control Performance (BAL002) Standards of the North American Electric Reliability Council [81] mandate that grid frequency should be maintained within certain predefined limits to guarantee grid stability. Frequency regulation helps to serve this purpose. The fast ramping capability of BESSs makes them ideal candidates for providing frequency regulation. Federal Energy Regulatory Committee (FERC) order 755 [82] makes it mandatory for independent system operators (ISOs) and utilities to consider speed and accuracy while buying frequency regulation provides the recommendations for pay-for-performance. A variety of models are employed by different ISOs to comply with this FERC order. The model developed and implemented by PJM Interconnection has been used in this work.

PJM employs a two-part payment model for resources committed to providing frequency regulation. These are regulation market capability clearing price (RMCCP) and regulation market performance clearing price (RMPCP). The former rewards the resource based on the capacity committed to regulation while the latter depends on the actual performance of the resource. These two payments make up the total revenue generated by the resource (which translates to the BESS in this study) from the regulation market. The RMCCP credit for a given hour can be calculated as follows [83].

$$\text{RMCCP Credit} = q_{\text{reg}}(t) \times \eta_t \times \lambda_c(t) \tag{3.4}$$

where $q_{\text{reg}}(t)$ is the BESS dispatch based on hourly integrated regulation signal, η_t is the actual performance score, and $\lambda_c(t)$ is the RMCCP, at time t. On the other hand, the RMPCP is determined as follows.

$$\text{RMPCP Credit} = q_{\text{reg}}(t) \times \eta_t \times \beta_t^M \times \lambda_p(t) \tag{3.5}$$

where β_t^M is the mileage ratio at time t.

The calculation of the mileage ratio is explained as follows. Two distinct regulation signals are offered by the PJM for different types of resources. The RegA signal is designed for traditional resources and is a low-pass filtered area control error (ACE) signal. On the other hand, RegD is designed for faster responding resources like BESSs and is a high-pass filtered ACE signal. Then, the mileage ratio, β_t^M, is defined as:

$$\beta_t^M = \frac{\text{RegD Mileage}}{\text{RegA Mileage}} \tag{3.6}$$

where mileage can be defined as the movement requested by the regulation control signal.

Therefore, the total income of the BESS from the frequency regulation market, J_{reg}, can be expressed as follows.

$$J_{\text{reg}} = \sum_{t=1}^{T} [\eta_t q_{\text{reg}}(t)(\lambda_c(t) + \beta_t^M \lambda_p(t))] \tag{3.7}$$

3.2.4 Optimal Location

The proposed framework provides the flexibility of locating an optimal site that can maximize the economic benefits of the BESS. The revenue from the energy arbitrage application depends on the temporal price difference in electricity, which is indicated by the LMPs. The LMPs at each node of a system are influenced by several factors including the geographic location, variability of load, connectivity with the rest of the network, and the uncertainty associated with renewable energy generation. Hence, it would be more profitable to locate the BESS at a node with high variability in LMPs. It should be noted that most of the revenue is generated by the frequency regulation application, for which the signals remain unchanged across all nodes in the network as these are dictated by the Independent System Operators (ISOs) and do not vary locally. However, performing regulation alone is not sustainable as the regulation signal in most control areas does not display zero average power [84]. This implies that the storage device needs to participate in other application(s) to preserve the charge-discharge dynamics of the battery subject to its total capacity. In summary, the BESS can be located at nodes with high variability in LMPs if such provision is allowed for and if the effort leads to tangible benefits. The focus of this study is not on the siting aspect although it offers the flexibility of choosing an optimal location if the need arises.

3.3 Battery Degradation Cost

As batteries undergo charging and discharging repeatedly, they degrade by losing their active material. The degradation process reduces the life of the battery and hence the degradation cost should be considered as an operational cost while determining the revenue of a BESS for a more accurate estimate. Hence, a degradation cost model is developed in this study and incorporated within the optimization framework and is described in this section.

3.3.1 DOD Stress Model

The lifetime of batteries depends on two components: its cycle life and its calendar life. Cycle life quantifies the loss of battery life due to cycling, while calendar life quantifies the life loss due to aging. The development of a degradation cost model is accomplished in this study with the help of cycle life only. Calendar life is not considered as it has little effect on the day-to-day operation of the battery.

The cycle life of a battery depends on its DOD among other things. The degradation of a battery per cycle depends on the DOD stress factor and can be expressed as follows [85].

$$\Delta_c = (k_{D1} DOD^{k_{D2}} + k_{D3})^{-1} \tag{3.8}$$

where Δ_c is the degradation per cycle, and k_{D1}, k_{D2} and k_{D3} are constants whose values depend on the battery technology. The use of a Lithium Nickel Manganese Cobalt Oxide ($Li(NiMnCo)O_2$) or LMO battery is assumed in this work. The stress model for DOD may be different for different battery technologies. The relationship between DOD and the number of cycles until its end of life (EOL) is illustrated in Fig. 3.1.

In this study, it is assumed that the battery reaches its EOL when its maximum capacity reduces to 80% of its original capacity. It is widely accepted in the automotive industry for the batteries to be discarded when they have depleted 20% of their original capacity. However, some researchers have proposed the use of these second-life batteries to be used for stationary power applications [86–89]. While second-life batteries can be suitable candidates for some applications like transmission support and load following, they are not suited to provide services like spinning reserve and frequency regulation [86]. This study considers the participation of the BESS in providing frequency regulation service, and hence the assumption that the battery reaches its EOL after depleting 20% of its original capacity is justified.

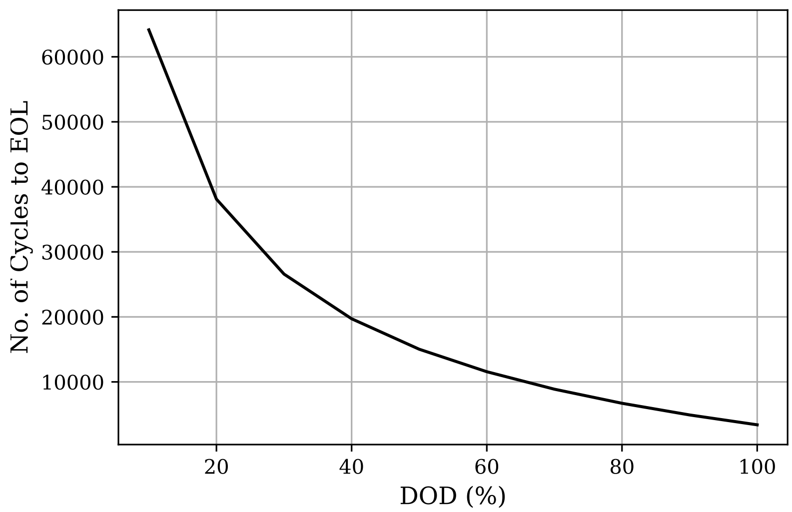

Figure 3.1: No. of cycles to EOL vs. DOD.

3.3.2 Degradation Cost Function

The degradation cost function of a BESS can be derived from its lifetime energy throughput [90], number of cycles, and the cost of the battery packs. First, a degradation cost coefficient, c_{deg} (\$/MWh), is defined as follows.

$$c_{\text{deg}} = \frac{c_{\text{bat}}}{E_{\text{ltp}}} \tag{3.9}$$

where c_{bat} is the battery cost and E_{ltp} is the lifetime energy throughput of the BESS. E_{ltp} can be defined as follows.

$$E_{\text{ltp}} = N_c \times \bar{S} \times \overline{DOD} \tag{3.10}$$

where N_c is the number of cycles the battery undergoes until its EOL, $\bar{S}$ the energy capacity, and $\overline{DOD}$ the average DOD of the battery. N_c is calculated for a particular $\overline{DOD}$ and varies as shown in Fig. 3.1. The relationship between the lifetime energy throughput and DOD is shown in Fig. 3.2. In this work, $\overline{DOD}$ has been assumed to be 80% to accommodate for the worst-case scenario since the SOC of the BESS is also restricted to 80% of the total capacity. In practice, not all cycles will have DOD as high as 80%. Hence, the results obtained by using this model will be conservative estimates of the actual values.

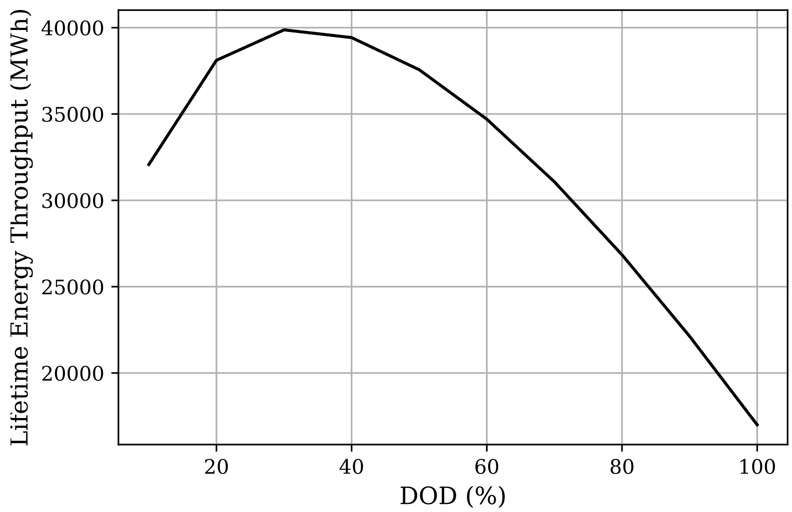

Figure 3.2: Lifetime energy throughput vs. DOD.

The degradation cost function, $C_d(t)$, is then derived from c_{deg} and the energy throughput of the battery for the time period t as follows.

$$C_d(t) = c_{\text{deg}} \times q(t) \tag{3.11}$$

where $q(t)$ is the total energy throughput from the BESS at time t. Since the BESS participates in the energy arbitrage and frequency regulation markets, the energy exchanged from these markets is the energy throughput from the BESS at any time t, and thus $q(t)$ can be expressed as:

$$q(t) = \eta_c q_r(t) + q_d(t) + (\eta_c \gamma_{\text{rd}}(t) + \gamma_{\text{ru}}(t)) q_{\text{reg}}(t) \tag{3.12}$$

Here, η_c is the round trip efficiency of the battery, γ_{ru} is the fraction of the regulation up reserve capacity actually employed at time t, and γ_{rd} is the fraction of the regulation down reserve capacity actually employed at time t.

3.4 Optimization Framework

This section describes the optimization framework for extracting the maximum economic benefits of the BESS. This framework includes the objective function, the network constraints, and the capacity and operational constraints for energy storage.

3.4.1 Objective Function

The objective of this framework is to maximize the BESS revenue by performing energy arbitrage and frequency regulation, and also to optimally locate the BESS. The revenue function, J can thus be expressed with the help of equation (3.2) as follows:

$$J = J_{\text{arb}} + J_{\text{reg}} - C_d \tag{3.13}$$

Therefore, the objective function can be expressed as:

$$\max \quad J = \sum_{n=1}^{N_{\text{bus}}} \left[\sum_{t=1}^{T} \lambda_{\text{lmp}}(t,n)[q_d(t)-q_r(t)] + \sum_{t=1}^{T}[\eta_t(\lambda_c(t)+\beta_t^M \lambda_p(t))q_{\text{reg}}(t)] - \sum_{t=1}^{T} C_d(t) \right] \tag{3.14}$$

where $\lambda_{\text{lmp}}(t,n)$ is the LMP at bus n for the time period t. The optimization framework is designed in a manner so as to calculate the revenue at each bus and automatically choose the bus with the maximum economic benefits by comparing their individual revenues.

3.4.2 Energy Storage Constraints

The operation of the energy storage is constrained by its physical capabilities, charging and discharging power limits, and cycle and self-discharge efficiencies. As the BESS charges and discharges every hour due to its participation in different applications, its remaining capacity changes every hour. The remaining capacity of a BESS is indicated by a metric known as the state of charge (SOC), which can be mathematically formulated as follows.

$$s(t+1) = \eta_s s(t) + \eta_c q_r(t) - q_d(t) + (\eta_c \gamma_{\text{rd}}(t) - \gamma_{\text{ru}}(t))q_{\text{reg}}(t) \tag{3.15}$$

where $s(t+1)$ is the SOC at time $(t+1)$. η_s is the self-discharge efficiency of the battery, γ_{ru} and γ_{rd} are calculated using historical data for PJM regulation signals [91, 92]. γ_{ru} and γ_{rd} are illustrated in Fig. 3.3 for a sample week.

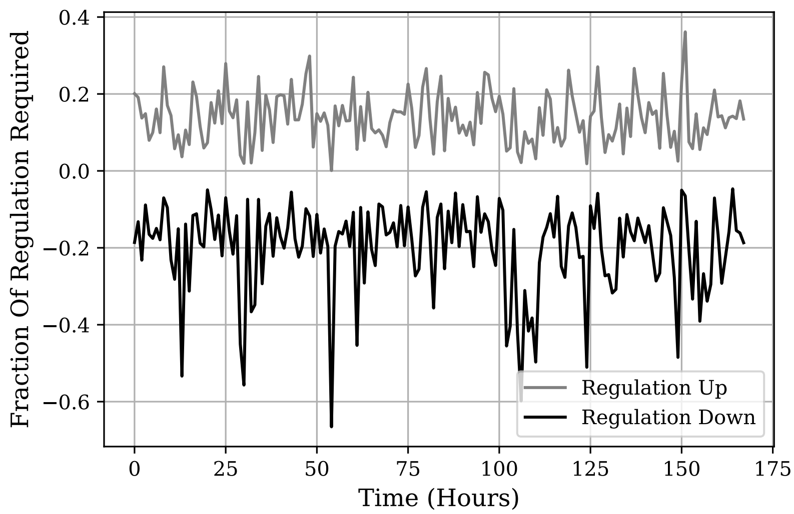

Figure 3.3: PJM regulation data for an example week.

The BESS operation is constrained by the following equations.

$$\gamma_{\text{reg}}^{\min} q_{\text{reg}}(t) + \gamma_s^{\min} \bar{S} \leq s(t+1) \tag{3.16}$$

$$s(t+1) \leq (1-\gamma_s^{\max})\bar{S} - \eta_c \gamma_{\text{reg}}^{\max} q_{\text{reg}}(t) \tag{3.17}$$

$$q_r(t) + q_d(t) + q_{\text{reg}}(t) \leq \bar{Q} \tag{3.18}$$

$$s(T) = s_0 \tag{3.19}$$

where, $\bar{S}$ is the BESS energy capacity in MWh; $\bar{Q}$ is the energy charge/discharge rating in MW and is derived from the power limit of the BESS; $\gamma_s^{\min}$ and $\gamma_s^{\max}$ are the fractions of energy capacity to be reserved for discharging and charging respectively; $\gamma_{\text{reg}}^{\min}$ and $\gamma_{\text{reg}}^{\max}$ are the fractions of regulation bid reserved for discharging and charging respectively. The γ_{reg} parameters ensure that the BESS meets all the regulation obligations and does not incur a penalty.

The minimum and maximum SOC limits are indicated by (3.16) and (3.17), respectively. Constraint (3.18) restricts the throughput based on the power rating while allowing charging and discharging during the same time step. The SOC level is maintained at the same level at the beginning of each day with the help of (3.19).

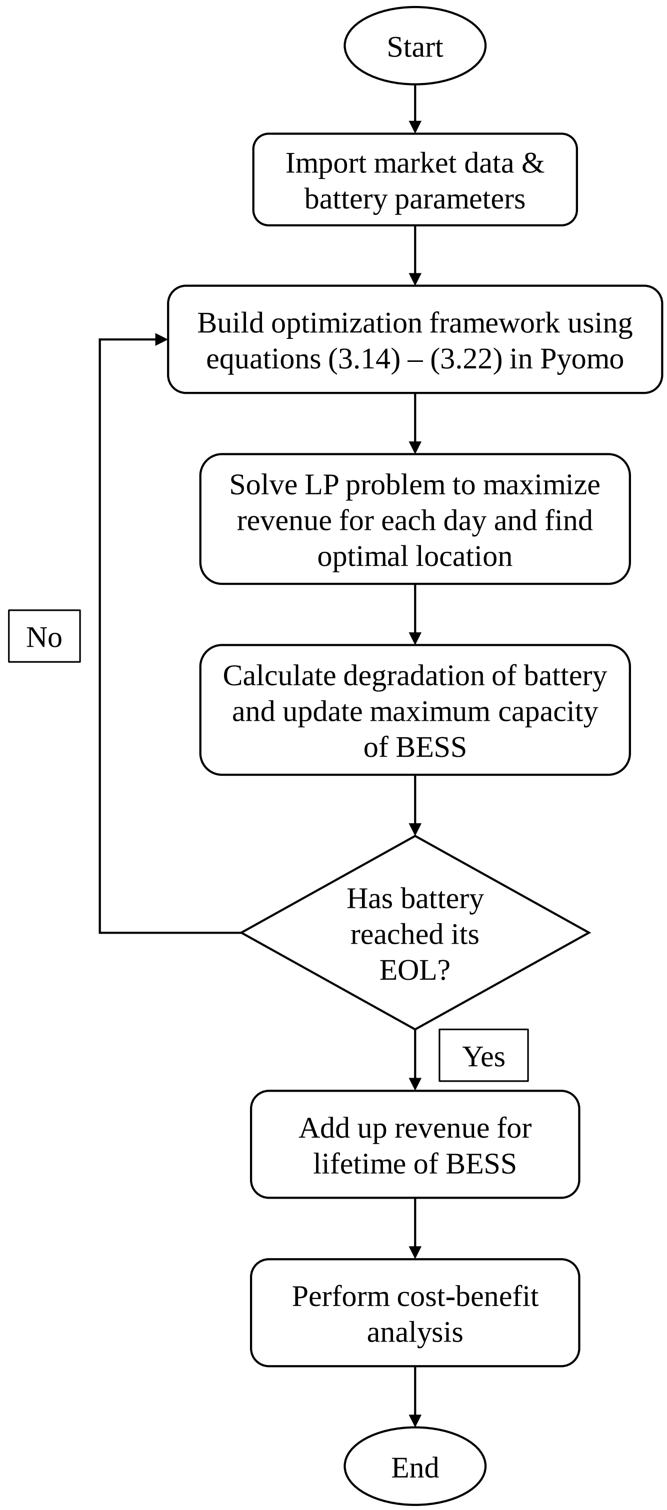

Figure 3.4: Flowchart summarizing the methodology used in the work.

3.4.3 Generation and Transmission Constraints

The network power flow is governed by generator limits, power balance, and transmission line constraints. A DC network model is applied in this research; as a result, the reactive power is neglected. The power flow in the network is constrained by the following equations.

- Power balance: The real power entering each bus n must equal the real power exiting it, at every instant of time t. The contribution of the BESS in the power exchange at each bus n is represented by the variables $q_d(t)$ and $q_r(t)$. It should be noted that the regulation variable q_{reg} is ignored as the regulation signal does not have any significant local effect. This constraint is modeled as follows.

$$P(t,n) = P_G(t,n) - P_L(t,n) + q_d(t) - q_r(t) \tag{3.20}$$

where

$$P(n) = \sum_{k=1}^{N_{\text{bus}}} B_{nk}\delta_k$$

$P(t,n)$, $P_G(t,n)$, $P_L(t,n)$ and are the real power injection, generation and demand at bus n at time t, respectively; B is the imaginary part of the admittance matrix, and δ_k is voltage angle of bus k.

- Generator constraints: The operation of each conventional generator is limited by its capability limit.

$$P_{\min}(g) \leq P(g) \leq P_{\max}(g) \tag{3.21}$$

where $P(g)$, $P_{\min}(g)$, and $P_{\max}(g)$ denote the minimum and maximum generation of the g^{th} generator. g is an index for the generators that ranges from 1 to N_g, the total number of generators in the system.

- Transmission line constraints: The transmission lines of the network are constrained by the amount of real power that can be transmitted.

$$|P_{kn}| = \left|\frac{(\delta_k - \delta_n)}{x_{kn}}\right| \leq P_{kn}^{\max} \tag{3.22}$$

Here, P_{kn} and x_{kn} are the real power transfer and the reactance between buses k and n, respectively, δ_k and δ_n are the voltage angles for buses k and n.

The decision variables in the proposed optimization framework are $q_d(t)$, $q_r(t)$, $q_{\text{reg}}(t)$, $P(g)$, δ_k and $s(t)$.

The methodology used in this work has been summarized in the flowchart, shown in Fig. 3.4.

3.4.4 Calculation of Lifetime Revenue

The lifetime revenue offered by the BESS is calculated by using the optimization framework described in the previous subsections. As the battery operates over time, it loses active material due to repeated charging and discharging. Hence, the maximum capacity of the battery decreases gradually.

In this work, the lifetime revenue is calculated using the method proposed in [93]. A semi-empirical degradation model is used to track the degradation of the battery and the maximum capacity of the battery is updated at regular intervals. The revenue is calculated and accumulated until the battery reaches its EOL.

3.5 Cost-Benefit Analysis

A life cycle cost-benefit analysis of BESS projects is performed in this study after obtaining the lifetime revenue as described in the previous sections. This analysis will enable investors in their decision-making process by providing them with an estimate of the net present value (NPV), the return on investment (ROI), and the payback period for the BESS projects.

3.5.1 Capital Cost

The total capital cost, C_0, includes the cost of the battery, power conversion system, the balance of plant, and other investment costs. The annualized capital cost C_{ACC} is calculated by multiplying the capital cost with the capital recovery factor (CRF). These quantities are determined as follows [94, 95].

$$C_0 = C_{\text{bat}} + C_{\text{inv}} + C_{\text{BOS}} + C_{\text{oth}} \tag{3.23}$$

$$C_{\text{ACC}} = C_0 \times \eta \tag{3.24}$$

$$\eta = \frac{i(i+1)^T}{(1+i)^T - 1} \tag{3.25}$$

where C_{bat}, C_{inv}, C_{BOS}, and C_{oth} represent costs of battery, battery central inverter, electrical and structural balance of system, and other investments including labor and tax, etc, respectively. η represents the CRF which is related to the interest rate i and the system lifetime T.

3.5.2 Replacement Cost

To accommodate the replacement costs for replaceable systems, e.g. batteries, the future cost of replacement and replacement period in years should be known. Annualized replacement costs can be calculated, given the number of replacements during the application lifetime, [95]. The annualized replacement cost, C_{ARC}, is calculated as follows.

$$C_{\text{ARC}} = C_{\text{RC}} \times [(1+i)^{-t} + (1+i)^{-2t} + \ldots + (1+i)^{-n_r t}] \times \eta \tag{3.26}$$

$$t = \min\left[T_{\text{cal}},\ T_{\text{cyc}}\right] \tag{3.27}$$

where C_{RC} is the replacement cost of battery, t is the replacement period, which is estimated with the degradation model in this study. t should be the calendar or cycle life of the battery, whichever comes first. n_r is the number of replacements during a certain period T.

3.5.3 Net Present Value

The net present value (NPV) for a BESS project is determined using the following equation.

$$\text{NPV} = -C_0 + \frac{C_1}{1+r_1} + \frac{C_2}{(1+r_2)^2} + \ldots + \frac{C_t}{(1+r_t)^t} \tag{3.28}$$

Here, C_t represents the net cash flow and r_t the discount rate for year t. The net cash flow is calculated as the revenue obtained from the market less the O&M costs.

3.5.4 Payback Period and ROI

The payback period represents the time required to recover the cost of an investment, while the ROI indicates the profitability of an investment over the lifetime of the battery. Unlike the NPV, when evaluating the ROI and payback period, the time value of money is not considered.

3.6 Results and Discussion

The approach proposed is validated using the IEEE Reliability Test System (RTS). The original system consists of 24 buses, 38 transmission lines, 5 transformers, and 32 generating units [64]. A single line diagram of this test system and all relevant system data are shown in Appendix B. Historical data from PJM Interconnection has been utilized for this study. PJM's Data Miner [96] has been utilized to obtain the RMCCP, RMPCP, mileage ratio, and the actual performance score for each hour. Data for one year starting from January 1, 2018, has been used. The parameters of the BESS utilized are shown in Table 3.1. The cost of a Li-ion battery has been assumed to be $209,000 per MWh [97].

Table 3.1: BESS parameters.

Parameter	Value
Power Capacity	10 MW
Energy Capacity	5–20 MWh
γ_s^{min}	15%
γ_s^{max}	5%
$\gamma_{\text{reg}}^{\text{min}}$	5%
$\gamma_{\text{reg}}^{\text{max}}$	5%
η_c	95%
η_s	95%

3.6.1 Revenue

The optimization framework presented in section 3.4 has been solved to obtain the annual revenue from the BESS. The BESS is optimized for the day-ahead market. Hence, the time horizon for the optimization problem is 24 hours $T = 24$. The revenue has been evaluated for three different sizes of BESS. The power capacity is maintained at 10 MW, while the energy capacity is varied from 5 to 20 MWh. Results are presented in tables 3.2 and 3.3 . These particular BESS sizes were selected as these are the most commonly used utility-size BESS in the U.S. and also represent short, medium, and long duration BESS [97].

Table 3.2: Lifetime revenue from BESS **considering** degradation cost.

Battery Size	Lifetime (years)	Revenue ($)	Mean cycles per year
10 MW, 5 MWh	6	8,116,541	1829
10 MW, 10 MWh	8	11,062,330	1731
10 MW, 20 MWh	10	13,139,466	1526

Table 3.3: Lifetime revenue from BESS **without considering** degradation cost.

Battery Size	Lifetime (years)	Revenue ($)	Mean cycles per year
10 MW, 5 MWh	5	10,492,202	2028
10 MW, 10 MWh	6	13,865,585	2072
10 MW, 20 MWh	8	17,629,318	1752

Upon observing the results presented in tables 3.2 and 3.3, it can be seen that neglecting the degradation cost of batteries leads to an overestimation of the lifetime revenue of the BESS. The average number of cycles undergone by the BESS per year is reduced when the degradation cost is considered, thus prolonging its lifetime. This observation holds true for all sizes of BESS used in the case studies and underlines the importance of considering the degradation cost while estimating the revenue of a BESS. Also, it can be observed that the lifetime revenue of longer duration BESS is higher than the shorter duration BESS due to the higher energy capacity of longer duration BESS.

The revenues generated by the individual applications were calculated to analyze the contribution of each application to the total revenue. It is found that most of the revenue is generated by the frequency regulation application. For example, for the 10 MW, 10 MWh BESS, frequency regulation contributes $2,348,109 for the first year, while the cumulative revenue from arbitrage was actually negative (-$2,942). However, it should be noted that performing regulation alone is not sustainable as the regulation signal in most control areas does not generate zero average power [84]. This implies that the storage device needs to participate in other application(s) to preserve the charge-discharge dynamics of the battery subject to its total capacity. Also, to participate in the more rewarding regulation market, the battery might sometimes need to be charged during periods of high LMPs which can lead to negative revenues from arbitrage. In summary, participating in the regulation market is extremely valuable for the BESS, but is not sufficient for technical reasons as explained.

3.6.2 Cost-Benefit Analysis

The results of the cost-benefit analysis are provided in this subsection. For the purpose of this analysis, only the case considering the degradation cost is included since the case without the degradation cost overestimates the revenue. Table 3.4 lists the annualized capital cost and annualized replacement cost. The project life is assumed to be 10 years in these calculations based on the calendar life of the battery [85]. The number of replacements is calculated based on the result of degradation analysis. There is no annualized replacement cost for the 10 MW, 20 MWh battery since its remaining capacity is larger than 80% at year 10, and thus no replacement is needed during the BESS project life.

The payback period, NPV, and ROI for different battery sizes are compared in Table 3.5. The fixed O&M cost is assumed to be 6 $/kW per year [98] while the discount rate r is assumed to be 5.5% [99]. The payback period represents the time required to recover the cost of an investment, while the ROI indicates the profitability of an investment over the lifetime of the battery. It should be noted that the time value of money is not considered while calculating the payback period and the ROI but is considered while calculating the NPV.

Table 3.4: Results of the annualized cost analysis.

Battery Size	Capital Cost ($/kWh)	Battery Cost ($/kWh)	Annualized Capital Cost ($)	Annualized Replacement Cost ($)
10 MW, 5 MWh	895	209	593,688	100,546
10 MW, 10 MWh	601	209	797,333	180,672
10 MW, 20 MWh	454	209	1,204,623	0

Table 3.5: Results of the life cycle cost-benefit analysis.

Battery Size	Payback Period (y)	NPV ($)	ROI (%)
10 MW, 5 MWh	3.5	2,041,521	80.6
10 MW, 10 MWh	4.5	2,441,298	83.4
10 MW, 20 MWh	6.5	510,846	44.0

From the results of Table 3.5, it can be observed that for larger BESS sizes, the payback period is longer and the NPV and the ROI are smaller. This can be attributed to the higher investment cost for larger BESS. Also, most of the revenue is generated by the frequency regulation application and BESS with smaller energy capacity and moderate power capacity are preferred for this purpose [84]. Hence, it can be concluded that the 10 MW, 5 MWh, and the 10 MW, 10 MWh BESS are better choices for investors due to their shorter payback period and higher NPV and ROI.

3.6.3 Effect of Uncertainty in LMPs on Revenue and Siting

Five sample paths of annual LMPs are generated to demonstrate the variation in revenue and optimal location. The results are presented in Table 3.6. The degradation cost is considered while calculating the annual revenue.

From the results, it can be observed that the variation in revenue due to uncertainty is very low. This is due to the fact that the revenue from energy arbitrage constitutes a very small portion of the total revenue. Also, the location remains unchanged due to the variability introduced in the LMPs.

Table 3.6: Variation in annual revenue & location for all sample paths.

Sample Path	Revenue ($)	Location. (Bus No.)
1	1,448,518	1
2	1,448,507	1
3	1,448,514	1
4	1,448,428	1
5	1,448,509	1

3.6.4 Modeling Language & Solver

Pyomo [100], a Python-based, open-source optimization modeling language is employed for modeling the problem. The objective function and the constraints in the proposed optimization framework are linear. Hence, the problem can be solved using any linear programming solver. *GLPK* has been used in this work.

3.7 Conclusion

This work proposes a new framework to maximize the economic benefits of a grid-connected battery energy storage system, by optimizing the annual dispatch strategy and location while also considering the degradation of batteries within the proposed framework. A general model is presented for the quantification of BESS revenue obtained from the electricity markets. Energy arbitrage and frequency regulation are chosen to be the applications in which the BESS participates due to their high profitability. A lithium-ion battery is the choice of the BESS for this study. The degradation cost of the BESS is taken into consideration for a more realistic estimate of the ROI. A new model for quantifying the degradation cost of batteries based on their lifetime energy throughput and the number of cycles is developed for batteries participating in the electricity markets and incorporated within the objective function. Results indicate that the inclusion of the degradation cost contributes to making the revenue estimate more realistic and accurate. Ignoring the degradation cost leads to the overestimation of the revenue. A comprehensive cost-benefit analysis is presented to provide an estimate of the ROI and the payback period. Results indicate that shorter duration BESS are better suited for market-related applications due to better ROI and shorter payback period when compared to longer duration BESS. The findings obtained by employing the proposed methodology can be utilized by investors and utilities during the planning phase of a BESS project and aid in the decision-making process based on the ROI and payback period.

CHAPTER 4

TECHNO-ECONOMIC PLANNING OF ENERGY STORAGE FOR INERTIAL SUPPORT IN WIND INTEGRATED SYSTEMS

4.1 Introduction

This chapter proposes a novel techno-economic planning framework that utilizes energy storage systems (ESSs) to maintain the frequency stability of the grid while minimizing the daily operating costs. Although the current U.S. electricity market structure does not support any mechanism to provide economic incentives or payback for synthetic inertia, it is possible that markets or other payment schemes can emerge as displacement of inertial generation increases and regulatory requirements evolve. For example, in 2011, Federal Energy Regulatory Commission (FERC) order 755 [82] mandated market operators to apply a pay-for-performance mechanism that reflects the speed and accuracy of the device being used for regulation and this led to the establishment of frequency regulation markets in several RTOs. Markets for ramping capability have also been established in the recent past [101]. In addition, some utilities such as Hydro-Quebec already mandate the use of synthetic inertia [102]. Therefore, it is not unlikely that synthetic inertia may become a necessary product in competitive markets in the recent future. Li *et al.* has proposed the design of a primary frequency control market for hosting frequency response reserve in collaboration with the Electric Reliability Council of Texas (ERCOT) in [103]. Our work anticipates these developments and proposes a techno-economic approach to size ESS for inertial support. The detrimental effects of reduced and often time-varying rotational inertia in the system can be reduced with the help of virtual or synthetic inertia [104]. Virtual inertia can be described as an imitation of the kinetic energy of synchronous generators used to improve system dynamical behavior [105].

Virtual inertia can be implemented by several means, one of the most widely discussed among these being the use of (ESSs) [11, 14, 16–19, 58, 106–110]. References [11, 14, 106] represent some of the earliest efforts that went into investigating the role of ESS in providing virtual inertial. These works mostly presented new modeling approaches for ESS providing inertial support and did not focus on the sizing aspect. References [16–19, 109], on the other hand, have proposed sizing approaches for ESS providing grid inertial support. Most of these works have focused on finding the minimum ESS size required to satisfy the inertia requirement of the system. Some of these works ([16–18, 109]) have also considered renewable energy penetration in their proposed solution methodology. However, in all of these works, the sole purpose of the ESS has been to provide virtual inertia to the system. In a practical power system, the ESS will be called upon for inertial support during certain disturbances, while it will be idle for the rest of the time. During this time, the ESS can be utilized to participate in market services where it can generate revenues to pay back some of its own investment cost or help in reducing the system operating costs. This work proposes to bridge this research gap. A new methodology based on estimating the system inertia is proposed, which not only offers the flexibility of sizing the ESS for the most extreme frequency events in a wind-integrated system but also allows it to participate in market services to generate revenues.

A bi-level stochastic optimization framework is developed to implement this strategy. The overarching objective of this framework is to minimize the daily operating cost of a power system while satisfying a frequency stability constraint. The lower-level problem seeks to minimize the production cost of electricity (economic dispatch), while the upper-level problem maximizes the revenue from the market. A bi-level formulation is necessary since the ESS needs to know how much capacity has to be reserved for inertial support before it can participate in the market. This is explained further in section 4.3. Energy arbitrage is used in this work to illustrate the participation of the ESS in the market, although the proposed framework can be easily modified to include other market applications like regulation or outage mitigation, as deemed suitable by the owner and/or the operator of the ESS.

The proposed framework is based on estimating the inertia of the system contributed by the participating generating resources. A frequency stability constraint is developed and incorporated into the optimization framework, which ensures that the ESS has enough reserves to supply the virtual inertia requirements of the system at any period. The virtual inertia requirement of the system depends on the equivalent inertia of the system and also the minimum inertia required to maintain frequency stability of the system at that period. A maximum frequency deviation limit derived from a generalized load frequency control (LFC) model is utilized to determine the minimum inertia required to maintain frequency stability under a certain disturbance. Wind power generation is modeled using an autoregressive moving average (ARMA) model, and the uncertainty in wind power generation is integrated into the optimization framework using a scenario tree structure. Several case studies are performed by varying the values of the system parameters to demonstrate the efficacy and flexibility of the proposed approach.

A summary of the contributions of this work is listed as follows.

1. A novel techno-economic planning framework based on estimating the system inertia is proposed, which not only offers the flexibility of sizing the ESS for the most extreme frequency events in a wind-integrated system but also allows it to participate in market services to generate revenues.

2. A bi-level stochastic optimization framework is developed, which estimates the system inertia and incorporates the uncertainties associated with wind power generation. This bi-level formulation is critical for estimating the system inertia, as information regarding the economic dispatch is necessary before committing the ESS for other grid services.

3. An estimate of the revenue from market participation of the ESS and the reduction in system operating costs is also presented. This cost analysis can benefit both investors and operators alike for making decisions related to the planning and operation of the ESS.

The remainder of this chapter is organized as follows. Section 4.2 describes the modeling of wind power output and integration of wind power uncertainty into the stochastic optimization framework. Section 4.3 presents the proposed bi-level optimization framework with all its components. Several case studies and their results are presented in Section 4.4 to demonstrate the efficacy of the proposed methodology, while some concluding remarks are provided in Section 4.5.

4.2 Stochastic Optimization and Wind Modeling

A stochastic optimization framework with a recourse model is used in this work. These models are widely used in operations research and are suitable for cases where some of the decisions must be fixed before information relevant to the uncertainties is available, while some of them can be delayed [111]. The former can be represented in terms of first-stage variables, and the latter by second-stage variables.

4.2.1 Recourse Model

In this work, the recourse model is utilized to incorporate the uncertainties of wind power generation. Dispatch decisions are made after observing the different possible outcomes of wind power generation to exploit the advantageous outcomes without becoming overtly vulnerable to the disadvantageous ones. A general form of the recourse model is presented as follows [111].

$$\mathbf{min}\ cx + E[h(x, \tilde{\omega})] \tag{4.1}$$

$$\text{s.t. } Ax \geq b \tag{4.2}$$

$$x \geq 0 \tag{4.3}$$

$$\text{where } h(x, \omega) = \mathbf{min}\ g_\omega y \tag{4.4}$$

$$\text{s.t. } W_\omega y \geq r_\omega - T_\omega x \tag{4.5}$$

$$y \geq 0 \tag{4.6}$$

Here, x is the first-stage decision and y is the second-stage decision. x does not respond to ω and is determined before any information regarding uncertain data has been obtained. y, on the other hand, is determined after observations regarding ω have been obtained.

4.2.2 Modeling of Wind Power Output

The power output of a wind farm is a function of the wind speed at that location. This section describes in detail the modeling of wind speed at a particular geographic location and hence the power output of wind farms.

4.2.2.1 Modeling of Wind Speed

Wind speed at a certain geographic location varies randomly with time. Hence, accurate models are needed to capture the various properties of wind speed. In this work, autoregressive moving average (ARMA) models are used to represent and forecast wind speed data.

In statistical time series analysis, ARMA models can provide a description of a stationary stochastic process using observations from previous time steps. ARMA techniques have been widely used by researchers to model wind speed due to their accuracy [52, 112, 113]. An ARMA model is a combination of an autoregressive (AR) model and a moving average (MA) model. The AR model predicts the value of a variable using the observations of the previous time steps while the MA model uses the residuals of the previous forecasts. The number of previous observations used by the AR and MA models decides the parameters p and q of the ARMA model, respectively. In general, the value of a variable y at time t can be forecasted using an ARMA(p, q) model as follows.

$$y_t = \phi_1 y_{t-1} + \phi_2 y_{t-2} + \ldots + \phi_p y_{t-p} + \epsilon_t + \theta_1 \epsilon_{t-1} + \theta_2 \epsilon_{t-2} + \ldots + \theta_q \epsilon_{t-q} \tag{4.7}$$

where ϕ_i and θ_j are the parameters of the AR and MA models respectively; ϵ is an independently and identically distributed (IID) white noise process and $\epsilon \sim N(0, \sigma)$. The forecasted wind speed at time t, FW_t can then be obtained as a function of y_t.

$$FW_t = f(y_t) \tag{4.8}$$

4.2.2.2 Modeling of Wind Turbine Output

It is necessary to convert wind speed data into wind power output data for modeling wind farms. This is accomplished using the following procedure. The power output of a wind turbine is a function of the wind speed as the turbines convert the kinetic energy of wind into electrical energy. The relationship between wind speed and wind power output is shown in (4.9) [52] and illustrated for a wind turbine of the rated power of 8 MW in Fig. 4.1.

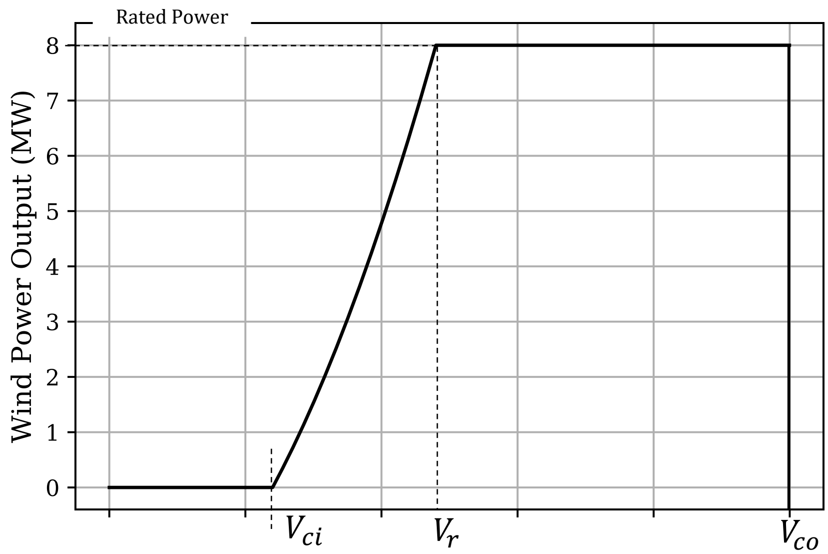

Figure 4.1: Typical relationship between wind speed and wind power output.

$$P_w = \begin{cases} 0 & 0 \le V \le V_{ci} \\ (A + B \times V + C \times V^2)P_r & V_{ci} < V \le V_r \\ P_r & V_r < V \le V_{co} \\ 0 & V_{co} < V \end{cases} \tag{4.9}$$

Here, V_{ci}, V_{co}, V_r, P_r are the cut-in, cut-out, rated speed, and rated power of the wind turbine, respectively. A, B, and C are constants defined as follows [114]:

$$
\begin{aligned}
A &= \frac{1}{(V_{ci} - V_r)^2}\left[V_{ci}(V_{ci} + V_r) - 4(V_{ci}V_r)\left(\frac{V_{ci} + V_r}{2V_r}\right)^3\right] \\
B &= \frac{1}{(V_{ci} - V_r)^2}\left[4(V_{ci} + V_r)\left(\frac{V_{ci} + V_r}{2V_r}\right)^3 - (3V_{ci} + V_r)\right] \\
C &= \frac{1}{(V_{ci} - V_r)^2}\left[2 - 4\left(\frac{V_{ci} + V_r}{2V_r}\right)^3\right]
\end{aligned}
$$

4.2.3 Scenario Tree Model

A recourse problem can be defined in terms of its scenario tree, which is used here to model the uncertainty in the outcome of wind power generation. The scenario tree represents the wind power outcomes in the order in which they may evolve over time and is used to make decisions on the recourse actions of the conventional units and the ESS. A nine-realization scenario tree similar to [115] is used in this work and is illustrated in Fig. 4.2. Each node of the tree represents a wind power outcome and the probability associated with that outcome. The required values at each node are determined using a quantile-based scenario tree technique [113]. Each branch of the tree represents a quantile, the values of which can be chosen by the operator. It should be noted that low quantile values represent negative forecast errors while high quantile values represent positive forecast errors.

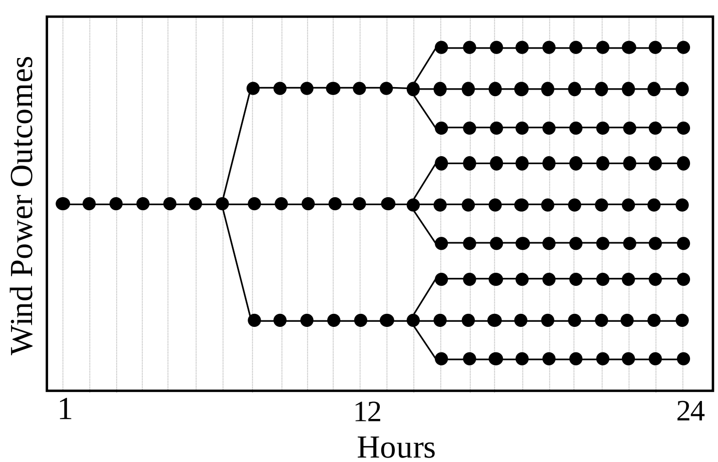

Figure 4.2: Nine-realization scenario tree representing the outcome of wind power outputs.

4.3 Bilevel Optimization Framework

A bi-level optimization framework is used in this work to determine the optimal ESS size required for maintaining frequency stability by providing virtual inertia. Bilevel optimization problems are hierarchical optimization problems which have two levels: *upper* and *lower*. The upper-level (UL) authority takes decisions subject to an optimal response from the lower-level (LL) authority. In other words, the feasible region of the UL problem is restricted by the graph of the solution set mapping of the LL problem [116].

A bilevel formulation is necessary for this problem due to the following reason. The amount of ESS capacity that can be committed to the electricity market at any particular hour is limited by the amount of energy it needs to reserve for providing grid inertial support (say q_t^{int}), which is its primary function. The quantity q_t^{int} can be determined once an economic dispatch is solved and the information regarding the committed generating resources is obtained. The inertia contribution from a generator for a particular time period is considered only if it is committed for dispatch at that particular hour. Hence, in the formulation presented in this work, the LL problem seeks to minimize the production cost of electricity and thus provides information regarding the committed generators, the total system inertia, and hence the value of q_t^{int}. The value of q_t^{int} is now fixed for the UL problem, which is then solved to decide the ESS capacity to be committed to the market and hence maximize its revenue.

The solution process of bi-level problems can be complex, computationally expensive, and often intractable. Under these conditions, the bi-level problem in this work is solved by considering the two levels independently. A linear solver is used for solving each level. This method ensures that the computational burden is low, while maintaining accuracy of the solutions.

4.3.1 General Mathematical Model

A general mathematical formulation of a bilevel optimization problem is shown here as follows [117].

$$
\begin{aligned}
&\textbf{min } f(x, y^*) \\
&\text{s.t. } g_1(x, y^*) \leq 0 \\
&\qquad h_1(x, y^*) = 0
\end{aligned}
$$

where

$$
\begin{aligned}
y^* \in &\textbf{ argmin } f_2(x, y) \\
&\qquad \text{s.t. } g_2(x, y) \leq 0 \\
&\qquad\qquad h_2(x, y) = 0
\end{aligned}
$$

Here, y^* represents the solution of the LL problem, which is used to determine the solution of the UL problem, denoted by $f(x, y^*)$.

4.3.2 Upper-Level Problem

The UL problem is formulated to maximize the revenue from the electricity markets. Energy arbitrage is used as an application for the ESS in this work, although the proposed framework can be easily modified to include other applications as well. A brief background regarding energy arbitrage is first provided.

Energy Arbitrage

Energy arbitrage is one of the oldest and most common applications of ESS. An ESS takes advantage of the temporal difference in the locational marginal prices (LMPs) to generate profits. It charges when the LMPs are low and sells energy by discharging when the LMPs are high. For this work, the inclusion of the energy arbitrage application is important for reasons both technical and economic.

First, participating in the electricity market through energy arbitrage helps the ESS in earning revenues which in turn offsets some of the investment and operating costs of the ESS. Second, only underfrequency events are considered in this work as they are more common and hence the ESS always discharges while providing inertial support. Participating in arbitrage allows the ESS to recharge after it has discharged, and it does so when prices are low.

4.3.2.1 Objective Function

The UL objective function can be expressed as follows.

$$\mathbf{min} \sum_{t=1}^{T} \lambda_t^{\mathrm{lmp}} \left(q_t^r - q_t^d \right) \tag{4.10}$$

where λ_t^{lmp} denotes the LMP at time t, while q_t^r and q_t^d are respectively the amount of energy charged and discharged from the ESS at time t.

4.3.2.2 Constraints

The UL objective function is constrained by the ESS capacity and operation constraints, and also by the proposed frequency security constraint. These constraints are listed as follows.

- *ESS SOC constraint:* The state of charge (SOC) can be defined as the remaining capacity of the ESS at any point of time. The SOC constraint ensures that the charge/discharge dynamics of the ESS is considered while calculating the remaining capacity at every time step and is expressed as follows.

  $$soc_t = \eta^s soc_{t-1} + \eta^c q_t^r - q_t^d - q_t^{\mathrm{int}} \tag{4.11}$$

  where η^s and η^c are the self-discharge and round-trip efficiencies of the ESS respectively. q_t^{int} is the amount energy that should be reserved for providing inertial support to the system at time t.

- *ESS operation constraints:* ESS operation is constrained by the following.

$$\gamma_s^{\min}\bar{S} \leq soc_t \leq (1-\gamma_s^{\max})\bar{S} \tag{4.12}$$

$$q_t^r + q_t^d + q_t^{\text{int}} \leq \bar{Q} \tag{4.13}$$

$$soc_T = s_0 \tag{4.14}$$

  where $\bar{S}$ and $\bar{Q}$ are the energy capacity and power rating of the ESS, and $\gamma_s^{\min}$ and $\gamma_s^{\max}$ are the fractions of energy capacity to be reserved for discharging and charging respectively.

- *Frequency stability constraint:* The modeling of grid frequency response, its relationship with system inertia and the contribution that an ESS can make toward frequency stability are described in detail in Section 2.4. Using the models present in that section, a frequency stability constraint is developed and presented here. This constraint ensures that the system inertia level remains above the minimum required to maintain frequency stability under a disturbance, and can be expressed as follows.

$$H_t^{\text{sys}} + H_t^{\text{ESS}} \geq H_t^{\min} \tag{4.15}$$

  where H_t^{sys} is the system equivalent inertia at time t and its value depends on the number of conventional units online. This information is obtained from the solution of the LL problem. If the power generation from a conventional unit is more than zero, then it is considered to be supplying full inertia to the system. H_t^{ESS} is the contribution of the ESS towards inertial support and $H_t^{\min}$ is the minimum inertia required to maintain frequency stability under a disturbance at time t.

4.3.3 Lower Level Problem

The LL problem is formulated to minimize the production cost of electricity. The LL problem follows a stochastic optimization formulation due to the introduction of wind energy. As explained in section 4.2, nine wind scenarios are considered in this work.

4.3.3.1 Objective Function

The cost function consists of the fuel cost of the conventional generators. The objective function of the LL problem can be mathematically expressed as follows.

$$\mathbf{min} \sum_{s=1}^{S} p_s \sum_{t=1}^{T} \sum_{i=1}^{G} C_{its}^{g} P_{its}^{g} \tag{4.16}$$

where C_{its}^{g} is the fuel cost and P_{its}^{g} is the active power generation of conventional unit i at time t in scenario s. p_s is the probability associated with scenario s, G is the number of conventional generators in the system, S is the number of scenarios considered, and T is the time horizon of optimization, which is one day or 24 hours in this work.

4.3.3.2 Constraints

The LL objective function is constrained by the network constraints of the system and the generator capacity limits. A linearized power flow model is used in this work. The constraints are briefly described as follows.

- *Power Balance:* The real power entering each bus n must equal the real power exiting it at time t for scenario s. This constraint is modeled as follows.

$$P_{nts} = P_{nts}^{g} - P_{nts}^{l} - P_{nts}^{w} \tag{4.17}$$

where

$$P_n = \sum_{k=1}^{nb} B_{nk} \delta_k$$

P_{nts}, P_{nts}^{g}, P_{nts}^{w} and P_{nts}^{l} are the real power injection, conventional generation, wind power generation, and demand at bus n at time t for scenario s, respectively; B is the imaginary part of the admittance matrix, and δ_k is voltage angle of bus k, and nb is the total number of buses.

- *Transmission line limits:* The transmission lines of the network are constrained by the amount of real power that can be transmitted.

$$|P_{kn}| = \left|\frac{(\delta_k - \delta_n)}{x_{kn}}\right| \le P_{kn}^{\text{fmax}} \tag{4.18}$$

Here, P_{kn} and x_{kn} are the real power transfer and the reactance between buses k and n, respectively, δ_k and δ_n are the voltage angles for buses k and n.

- *Generator limits:* The operation of each conventional generator is limited by its capacity limits.

$$P_i^{\min} \le P_i^g \le P_i^{\max} \tag{4.19}$$

where $P_i^{\min}$, and $P_i^{\max}$ denote the minimum and maximum capacities of generator i.

4.4 Case Studies and Results

Data from the New England IEEE 39-bus system [62] is used to test the efficacy of the proposed method. The original test system comprises 39 buses, 10 generators, and 46 transmission lines. A single line diagram of this test system and all relevant system data are shown in Appendix A. Part of the conventional generation is replaced by wind farms in some of the case studies presented in this work (elaborated in Section 4.4.1), to illustrate the effect of wind penetration on system inertia. Since load and wind patterns do not vary significantly over one particular season, one week from each season (28 days) is used for the daily operation model, and the yearly revenue is estimated from that. Time-of-use electricity prices are used for the LMPs [118] and fuel prices are obtained from [119]. The annual hourly load curve is obtained from [64] and adjusted according to the peak load of the test system. Data for the governor parameters are obtained from [56].

Uncertainty in wind power generation is modeled using the scenario tree illustrated by Fig. 4.2. The three branches of the tree represent the 0.05, 0.5, and 0.95 quantile of the distribution of forecast errors, respectively. It is assumed that the wind power generation forecast error follows a second-order auto-regressive or AR(2) model. Parameters of this model are obtained from [113].

4.4.1 Case Studies

The optimal planning approach proposed in this work is illustrated by three cases, by using varying degrees of wind penetration in each case. Disturbance in the form of a load of 0.1 p.u. is assumed to change the system frequency from its nominal value of 60 Hz. Minimum ESS sizes required to satisfy the frequency stability constraint are determined for three values of maximum frequency deviation (Δf_{max}), for each case. In general, the proposed approach can be used to size ESS devices for any value of maximum frequency deviation and any load disturbance. This provides the system operator with ample flexibility in choosing the parameters. Data for the inertia constant of wind farms are obtained from [58].

1. **Case 1:** The original system with only conventional generation is considered in this case.

2. **Case 2:** About 8% of the generation capacity of the system (the current share of installed wind capacity in the U.S. today) is replaced by wind generation. To achieve this, a conventional unit of 580 MW is removed from the system and replaced by a wind farm of capacity 640 MW. This wind farm is assumed to consist of 80 identical wind turbines, of 8 MW each.

3. **Case 3:** About 20% of the generation capacity of the system (target wind power share in the U.S by 2030 [30]) is replaced by a wind farm of capacity 1520 MW. Two conventional units with capacities of 646 MW and 865 MW are removed to achieve this.

4.4.2 Minimum Storage Required

The minimum amount of storage reserve required in MW ($P_{\text{min}}^{\text{ESS}}$) to satisfy the frequency stability constraint is shown in this section. Table 4.1 shows the different values of $P_{\text{min}}^{\text{ESS}}$ for the three cases. It should be noted that $P_{\text{min}}^{\text{ESS}}$ is determined in a way such that if an ESS of size $P_{\text{min}}^{\text{ESS}}$ is chosen, it should be able to deal with the even the most extreme cases of inertia shortage in the system for the pre-specified values of the disturbance and Δf_{max}. Results show that the ESS size required to satisfy the frequency stability constraint increases as wind generation increasingly

Table 4.1: Minimum storage required.

Case	$\mathbf{\Delta f_{max}}$ (Hz)	$\mathbf{H_{min}}$ (s)	$\mathbf{P^{ESS}_{min}}$ (MW)
1	0.085	734	205
	0.09	619	13
	0.095	531	N/A*
2	0.085	787	349
	0.09	659	136
	0.095	557	N/A*
3	0.085	875	509
	0.09	728	264
	0.095	608	64

*N/A indicates that ESS is not required for inertial support for this case

replaces conventional generators. This can be attributed to the low inertia contribution of the inverter-based wind resources. Also, it can be observed that for Cases 1 and 2 where there is low or no wind penetration, an ESS might not be required if $\Delta f_{\max}$ is set to a high value. However, from Case 3, it is evident that as wind penetration in the grid continues to increase, ESSs become necessary for inertial support.

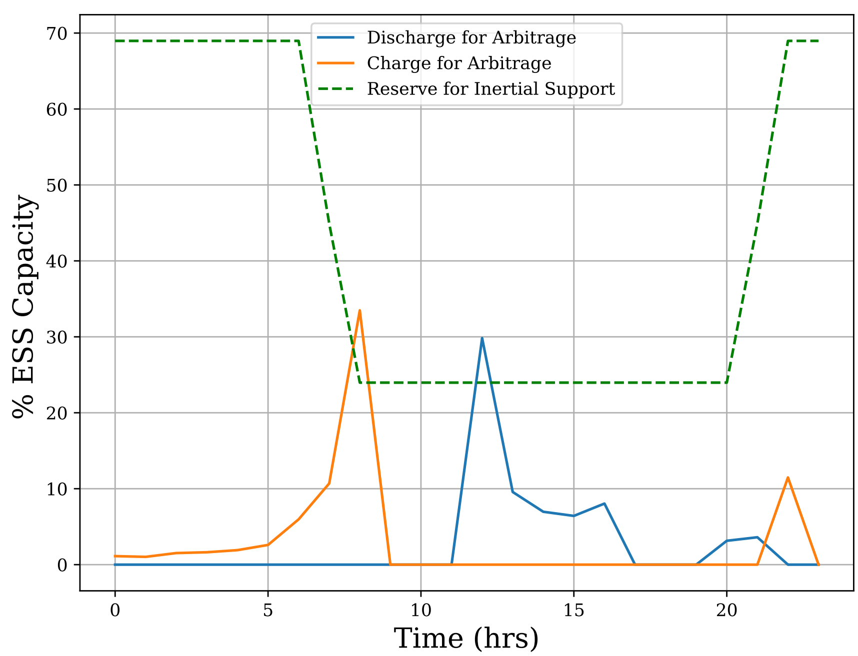

Figure 4.3: ESS operation for an example day (Case I).

Figure 4.3 illustrates the operation of the ESS for an example day for Case I. It shows how much energy the ESS charges or discharges for energy arbitrage or reserves for inertial support. One interesting observation from this figure is that the ESS reserves more energy for inertial support during the off-peak hours compared to the peak hours. This can be explained as follows. During peak hours, more generators are synchronized with the grid due to higher demand, thus maintaining a high level of system inertia. On the other hand, the system inertia is considerably lower during the off-peak hours since fewer generators are committed to serving the low demand. Hence, a higher amount of energy needs to be reserved for inertial support in the event of a disturbance for the low-demand periods.

Although the location of the ESS is not explicitly determined in this work, given that it is the wind farm that displaces system inertia, the ESS should be located near the wind farm for providing virtual inertia support. In case there are multiple renewable resources, the total ESS capacity required can be distributed proportionately among all locations containing the renewable resources.

4.4.3 Operating Cost and Revenue from Market

The ESS is considered to be performing energy arbitrage in this work, besides providing inertial support. Participation in the market service allows the ESS to recover some of the investment cost it incurs and thus reduce the daily operating cost of the grid. Although supplying inertia support does not generate any income at this point, it is possible that markets or other payment schemes can emerge as displacement of inertial generation increases and regulatory requirements evolve. A lithium-ion battery is used to illustrate the application of ESS in this work. The different parameters of the ESS used here are provided in Table 4.2.

The results of the economic analysis are shown in Table 4.3, which illustrates the revenue generated by the ESS from the market, the ESS investment cost, and the estimated value that can be recovered by the ESS from the market, as a percentage of the investment cost. For each case, it is assumed that $\Delta f_{\max}$ is 0.09, and 100 MW of storage in addition to $P^{\mathrm{ESS}}_{\min}$ is added to the system to

Table 4.2: ESS parameters.

Parameter	Value
Duration	1 hour
$\gamma_s^{\min}$	15%
$\gamma_s^{\max}$	5%
η^c	94.6%
η^s	98.5%
Investment Cost	\$ 601/kWh
Project Life	10 years

Table 4.3: Operating cost w. 100 MW additional storage.

Case	Production Cost (mil. \$)/day	Revenue (mil. \$)/yr	ESS Inv. Cost (mil. \$)	Est. Value Recovered (mil. \$)
1	1.95	1.94	67.9	19.4 (29%)
2	1.78	3.80	141.8	38.0 (27%)
3	1.65	4.45	218.8	44.5 (20%)

participate in energy arbitrage. For example, for Case 2, it is assumed that a 236 MW ESS is used. This number is used to illustrate the costs and the market revenue; ESS of a different size can also be used, according to the needs of the investors and the operators. Results show that using the ESS for energy arbitrage can recover a significant amount of the investment cost over the lifetime of the ESS project. This further justifies the utilization of the ESS for market services when it is not providing inertial support to the grid. The revenue from energy arbitrage will increase linearly as the size of the ESS used is increased. Results also show that the replacement of expensive conventional generation with cheap wind energy decreases the production cost. Investors and utilities may use the results presented here to decide on the size of the ESS they choose to acquire based on their requirements.

4.5 Conclusion

This chapter presents a novel optimal planning strategy for an ESS providing virtual inertia in a wind integrated system, emphasizing the techno-economic aspects of the problem. This planning strategy is implemented by developing a bi-level stochastic optimization framework with a recourse model, which minimizes the operational cost of the grid by participating in market services while satisfying a frequency stability constraint. The efficacy of the proposed methodology is successfully demonstrated using a lithium-ion battery as an example ESS, which is integrated into the IEEE 39-bus test system. The minimum amount of storage required to maintain frequency stability in the event of a disturbance is determined. Several case studies are performed which demonstrate the flexibility of the proposed approach in accommodating a wide range of system parameters while determining the optimal ESS size. The revenue generated from electricity markets is also determined, which can aid investors and utilities in deciding the size of the ESS according to their requirements. The proposed approach can also accommodate changes in future electricity markets providing economic incentives for virtual inertia, a situation becoming increasingly likely with more renewable energy resources replacing conventional generation.

CHAPTER 5

PLANNING FOR RELIABILITY IN WIND-RICH SYSTEMS USING STORAGE AND AGGREGATION

5.1 Introduction

Wind energy is one of the fastest-growing renewable energy resources used today for electric power generation. Sustained policy support and economic incentives for wind power generation across the world have led to its exponential growth in recent times [1]. However, this increasing penetration of wind energy is leading to reduced reliability and stability of the power grid due to its variable nature and non-dispatchable characteristics.

Transmission expansion offers several services to the grid, including aggregation of geographically diverse wind power. At the same time, there is increasing investment in ESS facilities due to their many applications, including firming up of wind power generation. In this chapter, we present a new transmission planning approach that jointly utilizes energy storage systems (ESSs) and wind aggregation to reduce wind variability and improve the reliability of the grid. This planning approach helps in overcoming the limitations of each individual method and provides a cost-effective solution to the wind variability problem. A probabilistic method is employed to determine the quantity of storage required to achieve a desired level of grid reliability. Extensive simulations are then performed to demonstrate how the storage required is reduced as a result of aggregating the outputs of geographically diverse wind farms. Congestion in the transmission system resulting from wind aggregation is also considered and is relieved by building new lines. The cost of building new transmission lines is compared to the cost of savings obtained due to the storage size reduction and it is observed that the proposed approach offers solutions that are less expensive than using storage alone. A replacement chain method is used to compare the net present values of the investments to offer a more accurate comparison of these investments which have different lifetimes.

The contributions of this work can be summarized as follows.

1. A transmission planning framework is developed for improving the reliability of wind-integrated systems by jointly utilizing energy storage and aggregation of geographically diverse wind power. This proposed approach helps to overcome the disadvantages of the individual methods and provides a cost-effective solution to the problem of wind variability.

2. Extensive simulation is performed to demonstrate the efficacy of the proposed approach in reducing the size of the ESS required to firm up wind generation. A detailed comparison between the cost of ESS and the cost of building new transmission is presented to demonstrate the cost-effectiveness of the proposed planning approach.

3. Composite system reliability assessment is performed to test the efficacy of the proposed planning strategy, considering the constraints of the transmission infrastructure, which are critical for aggregating wind power from different geographical locations.

The remainder of the chapter is organized as follows. Section 5.2 describes the approach used for the sizing of ESS to achieve a predetermined reliability target in a wind integrated system. Section 4.2.2 presents the modeling approach used for wind farms. Section 5.4 discusses the Monte Carlo techniques used and the reliability indices. Section 5.5 presents a mathematical model for the aggregation of wind power. Section 5.6 considers a few case studies and presents their results, while section 5.7 provides some concluding remarks.

5.2 Energy Storage Sizing

One of the main objectives of this work is to demonstrate how the aggregation of wind power leads to a reduction in the size of an ESS required to improve the reliability of the grid. Hence, it is only reasonable to set a reliability target and investigate how the combination of storage and aggregation can help the system to achieve that target. For this purpose, a probabilistic approach is used in this work to size the ESS [27]. It is important to note here that the ESS sizing technique presented in this chapter is different from the one presented in Chapter 2. In Chapter 2, the ESS is sized to provide inertial support to the grid for maintaining frequency stability, while the principal goal of the work presented in this chapter is to determine the size of an ESS required to achieve a pre-specified reliability target.

Let us assume that the availability of a wind-integrated system is A_0, and we need to increase its availability to A_1 using storage. Let us define a metric which we call unavailability reduction ratio, α, as follows.

$$\alpha = \frac{1 - A_1}{1 - A_0} \tag{5.1}$$

where $A_1 > A_0$. Let us also assume that a part of the load curtailment, P_L, is due to the variability of wind power generation. P_L can be calculated as follows.

$$P_L = P_W - P_{\mathrm{CV}} \tag{5.2}$$

where P_W is the nameplate capacity of the wind farm and P_{CV} is its capacity value, where capacity value can be defined as the amount of additional load that can be served from the addition of a unit, while maintaining the existing level of reliability [50].

From the above discussion, it is clear that the ESS needs to support a load of size P_L to increase system availability from A_0 to A_1 for a certain amount of time, which we assume to be t_A. Now, power supply is interrupted when both the grid supply is down and the storage has been depleted. The probability of this event can be expressed as follows [27].

$$P\{L_s\} = \left(\int_{t_A}^{\infty} f_R(r)dr\right) P\{L_{\bar{s}}\} \tag{5.3}$$

where $L_{\bar{s}}$ is the event that load is curtailed in absence of the ESS, L_s is the event that load is curtailed in presence of the ESS, R is a random variable representing the down time of the supply, and $f_R(r)$ is the probability distribution function of R. It can also be inferred from (5.3) that $P\{L_s\}$ equals $1 - A_1$, and $P\{L_{\bar{s}}\}$ equals $1 - A_0$. Hence, the following relationship can be derived from (5.1) and (5.3).

$$\int_{t_A}^{\infty} f_R(r)dr = \alpha \tag{5.4}$$

Where the down time does not follow a canonical distribution, MCS can be used, and the following relationship is more suitable, as shown in [120].

$$\int_{0}^{t_A} r f_R(r) = (1 - \alpha)\overline{r} \tag{5.5}$$

If the interruption durations without the ESS are arranged in order of increasing magnitude and if $\overline{r}$ is the mean interruption duration, then the time for which the mean of all equal and shorter interruptions is closest to $(1 - \alpha)\overline{r}$ gives the estimate of t_A.

Equation (5.5) presents the basic expression that quantifies the ESS energy capacity required to improve the system availability from A_0 to A_1. However, in a practical world, ESS are not perfectly reliable, and that should be considered in the model. Let us assume that the ESS has an availability A_s. Then, the ESS must possess an energy capacity that allows it to supply a load P_L for time t_s, where t_s is expressed as follows.

$$t_s = \frac{t_A}{A_s} \tag{5.6}$$

Hence, the power capacity of the ESS should be at least P_L and its energy capacity should be at least $P_L t_s$ for improving the system availability from A_0 to A_1.

5.3 Wind Speed Modeling and Data

In this work, wind speed is modeled using ARMA models. Details involving the models used for wind speed and wind power output are described in Section 4.2.2.

Wind speed data for a number of locations in the Eastern Interconnect of the U.S. are collected from the National Renewable Energy Laboratory's (NREL's) Wind Prospector [63]. Three years of wind speed data, ranging from January 1, 2010, to December 31, 2012, is used for each location to generate the ARMA model for that particular location. An AR model, a special case of an ARMA model, is used to model wind speed data at different locations. AR models are preferred for their simplicity and ease of interpretation and an AR model of appropriate order can be used to replace ARMA models without loss of accuracy [112]. The AR(8) model used to forecast wind speed data for Lansing, MI, is shown in (5.7). The accuracy of the AR model is further demonstrated by figures 5.1 and 5.2, which respectively show the plots of the observed and the predicted wind speeds of Lansing and their respective autocorrelations.

$$\begin{aligned} y_t = {} & 0.9553y_{t-1} + 0.0028y_{t-2} - 0.0203y_{t-3} + 0.0202y_{t-4} \\ & - 0.0149y_{t-5} - 0.0082y_{t-6} + 0.0002y_{t-7} - 0.0029y_{t-8} + \epsilon_t \end{aligned} \tag{5.7}$$

where $\epsilon_t \sim N(0, 1.113)$. The means and standard deviations of the observed and predicted wind

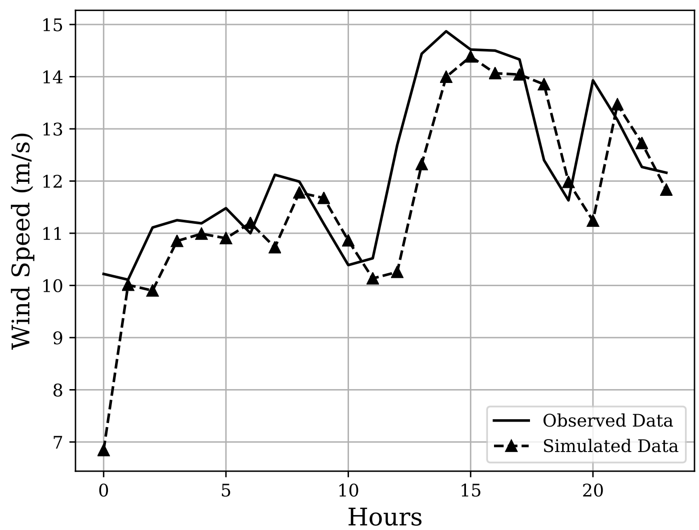

Figure 5.1: Observed vs. predicted wind speed for Lansing (one day).

speed data for a few other locations used in this work are shown in Table 5.1.

Table 5.1: Comparison between observed and predicted wind speed for different locations.

Location	Obs. Mean (m/s)	Pred. Mean (m/s)	Obs. Std. Dev.(m/s)	Pred. Std. Dev. (m/s)
Lansing, MI	6.84	6.77	3.21	3.08
Wash. DC	5.49	5.26	3.12	2.71
Omaha, NE	7.08	7.19	3.47	3.27
Flint, MI	6.75	6.72	3.17	3.04
Buffalo, NY	6.72	6.64	3.74	3.64
Richmond, VA	6.14	6.04	3.16	2.82
Atlanta, GA	5.87	5.73	2.95	2.66

Discussion on wind models used in this thesis: Readers might have noticed that two different wind models have been used in this thesis. In Chapter 2, a multi-state model is used, while in Chapters

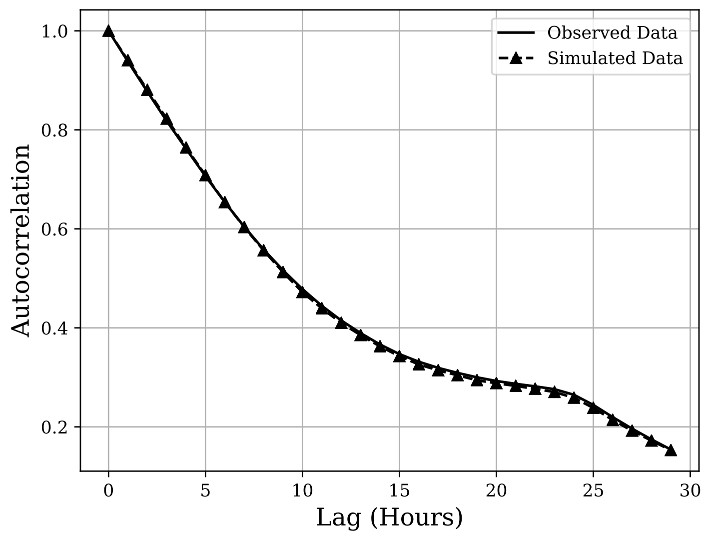

Figure 5.2: Autocorrelation of observed and predicted wind speed for Lansing.

3 and 4, an ARMA technique is used to model wind speed and wind power output. The reason for using multiple models is explained as follows.

In Chapter 2, an analytical model is used, which represents the wind farm as a multi-state generating unit with probability distributions of discrete capacity states, expressed in the form of a COPT. This enables the inclusion of the wind farm as a single, equivalent generating unit in traditional probabilistic planning methods. Chapter 2 presents an analytical approach for sizing ESSs for inertial support, and consequently, a multi-state analytical wind model is more suitable for such applications. On the other hand, an ARMA technique has been used to model wind speed and wind power output in Chapters 3 and 4. This approach allows to preserve the time-series nature of the wind speed and is more suitable for integration into simulation and optimization frameworks demanding sequential time-series data. Hence, this modeling approach has been used in Chapters 3 and 4, where simulation techniques have been employed for the optimization and evaluation of ESSs. In addition, ARMA models are also capable of accurately representing the autocorrelations between the different data points in a time-series dataset. This is particularly important for wind aggregation (used in this chapter), where the autocorrelations between the wind data from different geographical locations must be preserved to accurately reflect the benefits of aggregation.

5.4 System Reliability Model

Aggregation implies a heavier burden on the transmission lines and the effects of aggregation on the transmission system must be considered. Hence, composite system reliability analysis is performed in this work, taking into consideration the network constraints and the forced outages of the transmission lines. Sequential Monte Carlo simulation (MCS) is used to evaluate the reliability indices of the system. Sequential simulation is necessary to preserve the autocorrelation of the hourly wind speed model, which a non-sequential simulation might not be able to capture. The power system is represented by its components, which consist of conventional generators, wind turbine generators, transmission lines, and loads. Markov chains are used to model the components as two-state units, with the states being *up* and *down*. A brief description of the MCS algorithm is presented in the following section.

5.4.1 Mixed Timing Sequential MCS

Mixed timing sequential simulation combines both synchronous and asynchronous timing controls [47]. In its general form, mixed timing involves traversing an hourly load curve over a certain time period, and advancing the states of the system components asynchronously. This method can be implemented using the following steps.

1. Input failure rate and duration data for all components of the system.

2. Initialize all components in their *up* state.

3. Draw a random number for each component and calculate the time to the next event. The time to the next event for component i, T_i, is evaluated as follow.

$$T_i = -\frac{1}{\lambda_i} \ln(U_i) \tag{5.8}$$

   where U_i is a uniformly distributed random number and λ_i is the failure rate at the *up* state and the repair rate at the *down* state of the i^{th} component. Of these times, select the minimum time,

$T_{\min}(k)$. $T_{\min}(k)$ denotes the time to the most imminent event, i.e., after $T_{\min}$, component k changes its state.

4. At each hour, check the component capacities and if they are adequate to satisfy the load then no curtailment occurs. However, load curtailment may be required in case of a contingency. In such a scenario, load curtailment is minimized by using an optimization framework, and dispatch is rescheduled as explained in section 5.4.2.

5. Reliability indices are accumulated until a pre-specified convergence criterion is met. The system is said to have converged when an index attains a certain stable value. The stabilization of the value of an index i is measured by its standard error [121]:

$$\eta = \frac{\sigma_i}{\sqrt{n_c}} \tag{5.9}$$

where σ_i is the standard deviation of the index i and n_c is the number of simulated cycles. Convergence is said to have occurred when the standard error drops below a pre-specified fraction, ϵ, of the index i, i.e., when

$$\eta \leq \epsilon i \tag{5.10}$$

The simulation is said to have converged if the above criterion is satisfied.

5.4.2 Minimize Load Curtailment

Load curtailment might occur when one or more components of a system are forced into an outage due to some unforeseen circumstances. If such an event occurs, the system operators try to minimize the load curtailment and generate a viable dispatch. The minimization of load curtailment can be achieved through an optimization framework where the objective function is expressed as follows.

$$\min \; C_T = \left(\sum_{i=1}^{N_b} C_i \right) \tag{5.11}$$

where C_T is the total system load curtailment, C_i is the load curtailed at bus i, and N_b is the number of buses. This model ensures that power is rerouted within the network and the load curtailment is minimized in the event of a contingency. A positive value of C_T implies load curtailment, and an alternative dispatch is sought.

The objective function presented in (5.11) is constrained by generator capacity limits, power balance conditions, and transmission line limits. A linearized power flow model is used to construct the constraints in this work. The constraints are expressed as follows.

- *Power balance*: The real power entering each bus n must equal the real power exiting that bus. Thus, the power balance constraint can be expressed as follow.

$$P_n = P_n^G - P_n^L \tag{5.12}$$

where

$$P_n = \sum_{k=1}^{N_b} B_{nk}\delta_k$$

P_n, P_n^G, P_n^L and are the real power injection, generation and demand at bus n; B is the imaginary part of the bus admittance matrix, and δ_k is voltage angle at bus k.

- *Generator capacity limits*: The operation of each generator unit is limited by its capacity.

$$P_{min}^U \leq P_g^U \leq P_{max}^U \tag{5.13}$$

where P_{min}^U and P_{max}^U denote the minimum and maximum capacity of the g^{th} unit, and g ranges from 1 to N_g, the total number of units in the system.

- *Transmission line limits*: The transmission lines of the system are constrained by the amount of real power that can be transmitted over each line.

$$\left|\frac{(\delta_k - \delta_n)}{x_{kn}}\right| \leq P_{kn}^T \tag{5.14}$$

where P_{kn}^T and x_{kn} are the maximum capacity and the reactance between buses k and n, respectively; δ_k and δ_n are the voltage angles for buses k and n.

- *Constraint on curtailment*: The total curtailment must be less than or equal to the total system load, hence:

$$C_T \le \sum_{n=1}^{N_b} P_n^L \tag{5.15}$$

5.4.3 Reliability Indices

In this work, we have employed some commonly used indices for assessing the reliability of the system. These indices are briefly described below [47].

- *Loss of Load Probability (LOLP)* represents the probability of encountering one or more loss of load (LOL) events within a given time horizon.

- *Loss of Load Frequency (LOLF)* represents the expected frequency of encountering one or more LOL events within a given time horizon.

- *Mean Down Time (MDT)* represents the average interruption duration of the system. It has previously been denoted by $\bar{r}$ in section 5.2. It can be estimated as follows.

$$\mathrm{MDT} = \frac{\mathrm{LOLP}}{\mathrm{LOLF}} \tag{5.16}$$

- *Expected Demand Not Served (EDNS)* denotes the sum of the products of the probabilities of the LOL states and the corresponding load curtailments and can be estimated as follows.

$$\sum_{x_i \in X_L} P\{x_i\} \times C\{x_i\} \tag{5.17}$$

  where $P\{x_i\}$ and $C\{x_i\}$ are the probability of occurrence of state x_i, and the system load curtailment in state x_i respectively, and X_L is the set of loss of load states.

5.5 Wind Power Aggregation

This section discusses the merits of aggregating wind power from a number of wind farms which are located in different geographical areas. The mathematical models related to aggregation are also discussed.

5.5.1 Mathematical Modeling

The main idea behind aggregating the power outputs of different wind farms is that aggregation would reduce the variability of wind power and improve the reliability of the system. This hypothesis can be proved mathematically if we can show that aggregation can reduce the variance of the total power output from different wind farms spread across geographical areas, under certain conditions. Let us assume that there are x wind farms, each wind farm subjected to different wind speeds and patterns. Let each wind farm have y identical wind turbines with the output of the i^{th} wind farm being P_i^f. The total output power from all x wind farms, or the global output power, can then be expressed as follows.

$$P^{\text{Global}} = \sum_{i=1}^{x} P_i^f \tag{5.18}$$

The variance of this global power output is then given as follows [35].

$$\text{Var}[P^{\text{Global}}] = \sum_{i=1}^{x} \text{Var}[P_i^f] + 2\left[\sum_{i<j} \text{Cov}[P_i^f, P_j^f]\right] \tag{5.19}$$

where Var[·] and Cov[·] represent the variance and covariance operators, respectively. The first term represents the sum of variances of individual wind farms, and the second term the covariances between the power outputs of pairs of wind farms. Now, if we consider Pearson's correlation coefficient for the power outputs of a pair of wind farms, we see that it depends on their covariance.

$$\text{Corr}[P_i^f, P_j^f] = \frac{\text{Cov}[P_i^f, P_j^f]}{\sqrt{\text{Var}[P_i^f]\text{Var}[P_j^f]}} \tag{5.20}$$

From (5.19) and (5.20), we get:

$$\text{Var}[P^{\text{Global}}] = \sum_{i=1}^{x} \text{Var}[P_i^f] + 2\left[\sum_{i<j} \text{Corr}[P_i^f, P_j^f]\sqrt{\text{Var}[P_i^f]\text{Var}[P_j^f]}\right] \tag{5.21}$$

which implies that if the correlation coefficient between the outputs of two wind farms decreases, the variance of the global power output also decreases.

5.5.2 Role of Aggregation in Reducing the Size of the Storage

As shown in the previous section, aggregating the outputs of geographically diverse wind farms leads to a reduction in the output variability. It is reasonable to assume here that this will lead to an improvement in system reliability. Hence, the ESS size required to achieve a pre-specified reliability target would also reduce, when compared to the scenario where all the wind power is located at a single location. Let us assume that an ESS of size P_1 MW and $P_1 t_1$ MWh can firm up a single wind farm, and an ESS of size P_2 MW and $P_2 t_2$ MWh is required when wind power is aggregated from multiple wind farms. Then, $P_2 t_2$ should be smaller than $P_1 t_1$. It should be noted that the total nameplate capacity of the wind farms should be equal for the two cases, for the purpose of comparison.

5.6 Case Studies & Results

The efficacy of the proposed planning strategy is validated using a modified version of the IEEE Reliability Test System (RTS) [64]. This section describes the test system, some case studies and their results, followed by detailed analysis and discussion of the results.

5.6.1 Test System

The original system consists of 24 buses, 38 transmission lines, 5 transformers, and 32 generating units [64]. A single line diagram of this test system and all relevant system data are shown in Appendix B. The transmission network in the original system was found to be highly reliable and hence not suitable for demonstrating the effects of wind aggregation on the loading of the transmission lines that might lead to congestion. Hence the original system was modified by multiplying the total generating capacity of the system by a factor of 2, and the demand by a factor of 1.8 [122]. The total installed capacity of this modified system is 6810 MW, with a peak load of 5700 MW. A single line diagram of the test system is presented in Fig. 5.3. The lengths of all transmission lines are multiplied by a factor of 10 so that the locations simulated at the different buses are sufficiently separated to experience diverse wind patterns.

The system is further modified by adding wind farm(s) of capacity 1700 MW (which is about 20% of the total installed capacity, the target share of installed wind capacity in the U.S. by 2030 [30]) to simulate the effects of wind aggregation, the details of the case studies being provided in Section 5.6.3. Each wind farm is assumed to comprise of multiple Vestas V-150 wind turbine generators [123] rated at 4 MW each, the number of wind turbines depending on the total nameplate capacity of the wind farm. This particular turbine is chosen since it is designed for the International Electrotechnical Commission (IEC) III-B (low wind) wind class, which is consistent with the data used in this work, as shown in section 5.3. The forced outage rate (FOR) of wind turbine generators (WTGs) are assumed to be 0.08 [124].

5.6.2 Reliability Target

As mentioned in section 5.2, the ESS is sized in this work with the goal of achieving a pre-specified reliability target. This reliability target is determined in terms of the unavailability reduction ratio, α, which is calculated using the following steps.

1. A wind farm of capacity 1700 MW is added to the original test system and the LOLP is calculated.

2. The wind farm is replaced by a conventional generator of the same capacity and the LOLP is recalculated. This is the target LOLP of the system.

3. The unavailability reduction ratio α can be determined from the ratio of the target LOLP and the LOLP of the wind-integrated system, as explained in [28].

5.6.3 Case Studies

The following case studies are performed to show the reliability improvement of the system and the reduction of ESS size due to aggregation.

- **Case I**: Wind farms of total nameplate capacity 1700 MW (could be a single or multiple wind farms but are subjected to the same wind profile) are considered at a single bus in the system; the reliability of the system is evaluated, and the ESS size required for achieving the reliability target is calculated.

- **Case II**: Wind farms of nameplate capacities 850 MW each are considered at two different buses in this case. The wind farms at the two different buses have different wind profiles and help in simulating the geographical diversity between two locations. The wind power outputs at these two buses are then aggregated to study the effect on system reliability and ESS size. The effect of correlation between the two wind profiles on aggregation is also studied. The Lansing wind profile is considered for one bus (Location 1), while the wind profiles from Omaha, Buffalo, and Flint are considered for the other bus (Location 2).

Note on Siting of Wind Farms: In general, a suitable site for building a wind farm is selected based on several factors, including the wind profile, load demand, distance from load centers, cost of building the project, distance from nearby airports, and land availability. Siting of wind farms is not the primary focus of this work, and hence it is assumed that wind power is aggregated from existing wind farms, instead of building new ones at favorable locations. It is assumed that the wind farms are located at buses 3 and 19 since these buses are connected to significant amounts of load and are in close proximity to other load buses.

5.6.4 Results

The results obtained by employing the proposed strategy are provided here. Table 5.2 presents the reliability indices obtained for the original system, and by adding a 1700 MW conventional generator. The latter is necessary for calculating the reliability target, as explained in section 5.6.2.

Table 5.3 shows the reliability indices obtained by adding wind power of nameplate capacity 1700 MW to a single bus (bus 19) using the Lansing and Washington DC wind data, respectively. The sizes of ESS required to achieve the reliability target are also shown in this table.

Table 5.2: Reliability indices for the Base Case.

Case	LOLP	LOLF (f/yr)	MDT (h/yr)	EDNS (MW/yr)
Base	0.006400	6.19	9.06	0.8552
Conv.*	0.004283	2.66	14.11	0.4988

*Conventional unit of capacity 1700 MW added to test system

Table 5.3: Results for Case I.

Wind Profile	LOLP	LOLF (f/yr)	EDNS (MW/yr)	P_L (MW)	t_s (h)
Lansing	0.006064	5.56	0.7993	1459	3.35
Wash. DC	0.006156	5.93	0.8035	1586	3.33

Table 5.4 shows the results of aggregating wind power from two different locations having two different wind profiles. The Lansing wind profile is chosen for bus 19 (Location 1), and wind power of nameplate capacity 850 MW is added to this bus. Wind power of nameplate capacity 850 MW is added to bus 3 (Location 2) and the wind profiles of Omaha, DC, Buffalo, and Flint, are used at this bus. The wind profiles for Location 2 are chosen based on their correlation with the wind profile at Location 1 (low, medium, and high correlation). Comparing the results presented in Tables 5.3 and 5.4, it can be observed that the reliability of the system has improved due to aggregation.

In general, as observed from the results presented in Table 5.4, the reliability improvement is higher when the correlations between the wind profiles of the two candidate locations are lower. This is because wind farms with higher correlation in their power outputs are most likely subjected to similar wind patterns and hence the benefits of aggregation are less. However, lower correlations between the wind profiles of the two locations do not always result in higher reliability improvement. For example, when the DC wind profile is used at Location 2, the reliability improvement of the system is lower as compared to when the wind profiles of Buffalo and Flint are used, although the correlation between the Lansing and DC wind profiles is lower than the other two. This is because the degree of reliability improvement also depends on the mean wind speed of the different locations. From Table 5.1, it can be observed that the mean wind speed of DC is significantly lower than that of Buffalo or Flint, thus resulting in a reduced reliability improvement.

Table 5.4: Results for Case II.

Location 2*	Correlation	LOLP	LOLF (f/yr)	EDNS (MW/yr)	P_L (MW)	t_s (h)
Omaha	0.1207	0.005416	4.81	0.7008	1433	2.33
DC	0.1626	0.005777	5.64	0.7514	1522	2.72
Buffalo	0.4969	0.005666	5.22	0.7348	1450	2.69
Flint	0.8649	0.005713	5.32	0.7439	1463	2.74

*Lansing Wind Profile at Location 1

Results show that the ESS sizes required to achieve the reliability target decrease when wind power is aggregated. For instance, 1459 MW, 4888 MWh of storage is required when all wind power is located at a single bus. On the other hand, when wind power between the two locations is aggregated, a storage size of 1450 MW, 3901 MWh is enough to achieve the reliability target (Buffalo wind profile at Location 2). Similar results are obtained for all simulated cases for both cases II-A and II-B.

5.6.5 Cost Analysis of Proposed Approach

One disadvantage of aggregating wind power over different geographical locations can be the congestion of transmission lines. This aspect is investigated in this section and a detailed analysis is provided to show how the proposed strategy is cost-effective despite line congestion.

Let us consider the case where we assume the Lansing wind profile at Location 1 and the Buffalo wind profile at Location 2 (third row of Table 5.4). Aggregating the wind power from these two locations leads to congestion in four lines, indicated by A, B, C, and D in Fig. 5.3. The lengths of these congested lines are provided in Table 5.5. New transmission lines are then added

Table 5.5: Congested line lengths.

Line	A	B	C	D
Length (miles)	220	310	160	150

to the system to relieve this congestion. Different cases are simulated by adding a single line or a combination of lines to investigate the reliability improvement and the change in ESS costs required to meet the reliability target. Lithium-ion batteries are selected for the ESS due to their high energy

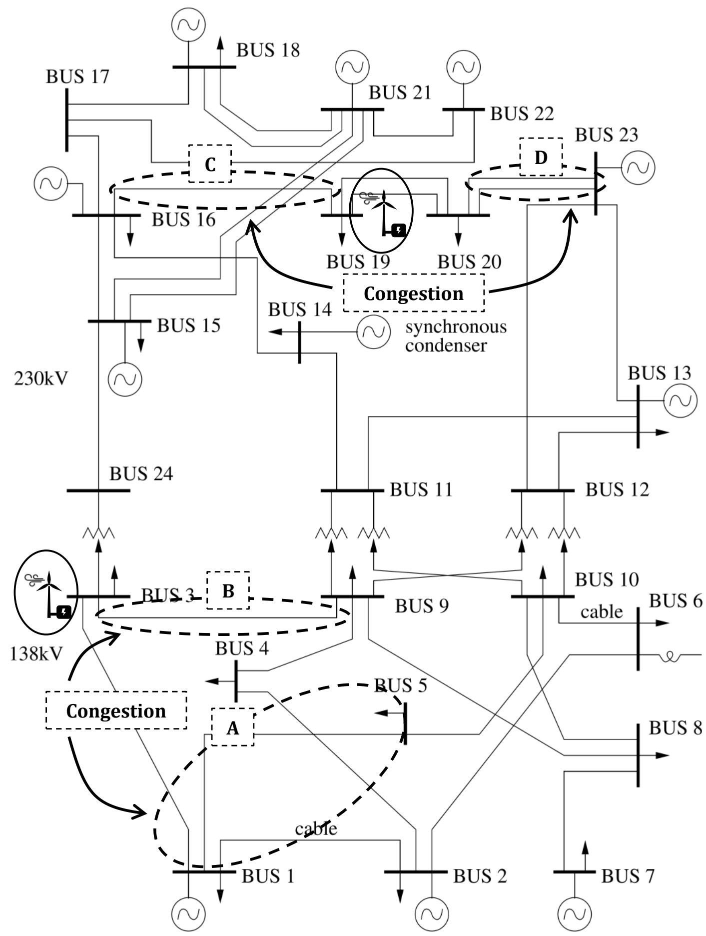

Figure 5.3: Congestions in the IEEE RTS due to aggregation of wind power.

density, high ramp rates and decreasing costs. Results are shown in Table 5.6. Cost considerations are shown in Table 5.7 [97, 125, 126] and the results are also illustrated in Fig. 5.4 to demonstrate the cost-effectiveness of the proposed planning approach.

Table 5.6: Results of adding new transmission lines.

Addl. Lines	New LOLP	ESS NPV (mil. $)	Trans. Line NPV (mil. $)	Total (mil. $)
B	0.005620	2383.98	274.48	2659
B,C	0.005551	2271.06	513.98	2785
A, C, D	0.005213	1576.16	660.65	2237
A, B, C	0.005172	1506.67	710.60	2217

Results show that adding new overhead transmission lines decreases the size and hence cost of storage required to meet the reliability target. New transmission lines incur additional costs and the

Table 5.7: Cost considerations for ESS and transmission lines.

Item	138 kV Line	230 kV Line	Line O&M	ESS Invest.	ESS Repl.	ESS O&M
Cost	\$ 0.823 mil. /mile	\$1.536 mil. /mile	\$22,000 /mile/yr	\$454 /kWh	\$209 /kWh	\$10 /kW-yr

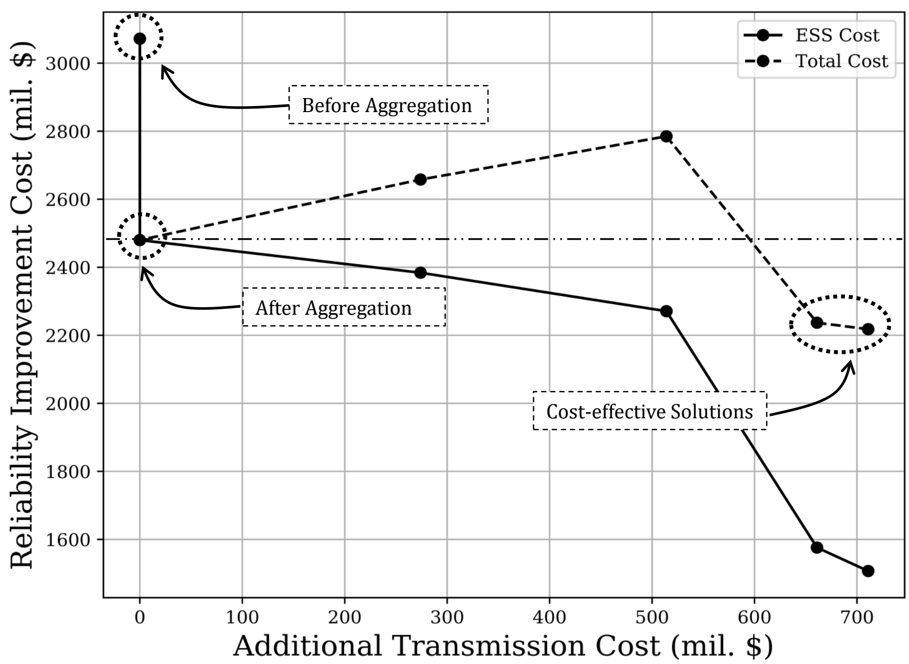

Figure 5.4: Cost of using ESS alone vs. the cost of employing the proposed strategy.

total cost of ESS and transmission lines initially increases. However, as more new lines are added, the total cost decreases and it eventually becomes lower than the cost of using ESS alone to achieve the reliability target.

All costs shown in Table 5.6 are the Net Present Values (NPVs) of investments using a replacement chain method. The replacement chain method offers a more accurate way of comparing projects with different lives. The lifetime of a transmission line is considered to be 30 years and that of an ESS project to be 10 years [125]. NPV adjusts for inflation, depreciation, and taxes. While calculating NPVs, a tax rate of 20%, a Weighted Average Cost of Capital (WACC) of 10%, and inflation of 2% are assumed.

5.6.6 Discussion

The results presented in Section 2.5 illustrate the efficacy of the proposed planning approach. Using extensive simulations it is demonstrated that aggregation of geographically diverse wind power indeed reduces the storage quantity needed to achieve a desired reliability target (Tables 5.3 and 5.4). As expected, the transfer of significant amounts of wind power led to congestions in some lines; this is indicated in Fig. B.1. The mitigation of such congestion requires the construction of new transmission, which is also expensive. Table 5.6 shows the costs of transmission additions for the cases considered. We have shown that an integrated planning approach to storage deployment and transmission expansion can lead to significant savings (see Fig. 5.4).

Yet another application of the proposed planning approach is the following. An analysis performed in 2008 by the U.S. Department of Energy [30] showed that much additional transmission was required in the U.S. to accommodate 20% wind by 2030. Regional Transmission Organizations (RTOs) and NERC (North American Electric Reliability Corporation) Regions routinely conduct transmission expansion studies, and some of these plans have already been implemented in recent years. Coordination with these expansion plans by utilities planning on constructing energy storage installations can lead to savings in the cost of these installations, and this constitutes another potential use case of the proposed method.

5.7 Conclusion

RTOs and other entities invest in transmission expansion for several reasons, including that of enabling aggregation of wind power. Concomitantly, utilities have been investing in storage facilities for many reasons, including mitigation of wind variability. This work presented an integrated planning strategy to optimize the costs of transmission and storage, using a probabilistic framework, and a uniform project valuation approach (i.e., the NPV) to account for the disparate time frames of transmission and storage projects. Results showed that aggregation of geographically diverse wind reduces the quantity and hence the cost of storage required to achieve a desired reliability target. Although the proposed strategy might lead to an additional cost of constructing new transmission lines for congestion relief, this cost is offset by the savings obtained due to the reduced storage size, eventually resulting in a lower overall cost. Consequently, this proposed integrated strategy can be employed by utilities planning on energy storage installations and transmission expansions in wind-rich systems to generate significant cost savings in their investments.

CHAPTER 6

CONTRIBUTIONS AND FUTURE WORK

6.1 Research Contributions

This thesis investigated the role of energy storage systems (ESSs) in alleviating some of the most critical issues faced by the modern power grid due to the integration of renewable energy resources (RERs). Models were developed for the evaluation and optimization of ESSs as cost-effective means of improving the stability and reliability of RER-integrated systems. The contributions of this thesis are summarized here as follows.

1. An analytical approach is developed for sizing of ESS to provide inertial support. This analytical approach potentially paves the way for solving more complicated problems related to the frequency stability of the grid with less computational burden and complexity. It also brings together in its framework the two most common causes of reduced inertia in the system: generator outages and replacement of conventional synchronous generators with RERs.

2. A new method is developed for calculating the probability of synchronization of the generating resources of the power system, which is necessary to estimate the probability distribution of system inertia.

3. An equivalence is proved between the probability of synchronization and the capacity value of wind farms, which is necessary to calculate the participation of wind farms in providing inertial support to the grid.

4. A new framework is developed for a comprehensive investment planning study of grid-connected storage systems with the objective of maximizing economic benefits. This framework is capable of including multiple products (such as energy arbitrage and frequency

regulation) as well the battery degradation cost, along with a comprehensive set of operating constraints.

5. An improved degradation cost model for lithium-ion batteries participating in the electricity markets is developed and incorporated within the optimization framework. This new degradation cost model considers both the lifetime energy throughput and the cycle count of the batteries. It also considers the cost of the battery packs which reflects the cost of degradation in monetary units.

6. A new techno-economic planning strategy is developed for optimally sizing ESSs to alleviate frequency stability issues of a wind integrated system while minimizing the operational costs of the system by participating in electricity markets. This strategy is implemented with the help of a bi-level stochastic optimization framework, which estimates the system inertia and incorporates the uncertainties associated with wind power generation. This bi-level formulation is critical for estimating the system inertia, as information regarding the economic dispatch is necessary before committing the ESS for other grid services.

7. A transmission planning framework is developed for improving the reliability of wind-integrated systems by jointly utilizing ESSs and aggregation of geographically diverse wind power. This approach helps to overcome the disadvantages of the individual approaches and provides a cost-effective solution to the problem of wind variability. Extensive simulation is performed to demonstrate the efficacy of the proposed approach in reducing the size of the ESS required to firm up wind generation. A detailed comparison between the cost of ESS and the cost of building new transmission is presented to demonstrate the cost-effectiveness of the proposed planning approach.

6.2 Future Work

This thesis focused on some of the key issues of the modern power grid that can be alleviated using ESSs. The work presented in this thesis can be extended to further enhance the performance of the RER-integrated grid. A guideline on how future research can be conducted based on this thesis is provided here:

1. An analytical framework and a planning strategy for sizing of ESSs for grid inertial support are presented in this work. However, the siting of ESSs for this purpose has not been investigated in detail. The placement of storage in the grid can affect their contribution toward frequency stability. Hence, comprehensive planning frameworks and metrics need to be developed to maximize the contribution of ESSs by optimally siting them.

2. The reliability benefits of jointly deploying ESSs and wind power aggregation are investigated in this work. However, the transmission network also plays a crucial role in maintaining the stability of the grid. Hence, it would be interesting to see how the joint strategy can benefit the stability of the grid as well, in presence of increasing RER penetration.

3. The current US electricity market structure does not support any mechanism to provide economic incentives or payback for synthetic inertia. However, it is possible that markets or other payment schemes can emerge as displacement of inertial generation increases and regulatory requirements evolve. Hence, new frameworks should be developed for incorporating virtual inertia as a compensation-based service in the electricity markets, and new strategies should be devised for ESSs to optimally participate in these markets.

4. A new degradation cost model is proposed for lithium-ion batteries in this thesis, which considers both the lifetime energy throughput and the cycle count of the batteries. However, lithium-ion battery models are evolving at a fast rate as increasing quantities of these batteries are deployed in the grid. The more recent models of Li-ion batteries are being designed to represent the intricacies and complexities of battery dynamics to present a more accurate picture of their functioning. In this regard, battery degradation models should also be updated to incorporate these intricacies and to get more accurate estimates of the costs associated with such projects.

APPENDICES

APPENDIX A

IEEE 39-BUS TEST SYSTEM

This section provides the data used for the IEEE 39-bus test system, along with a single line diagram, as shown in Fig. A.1. This test system has been used in Chapters 2 and 4 of this thesis.

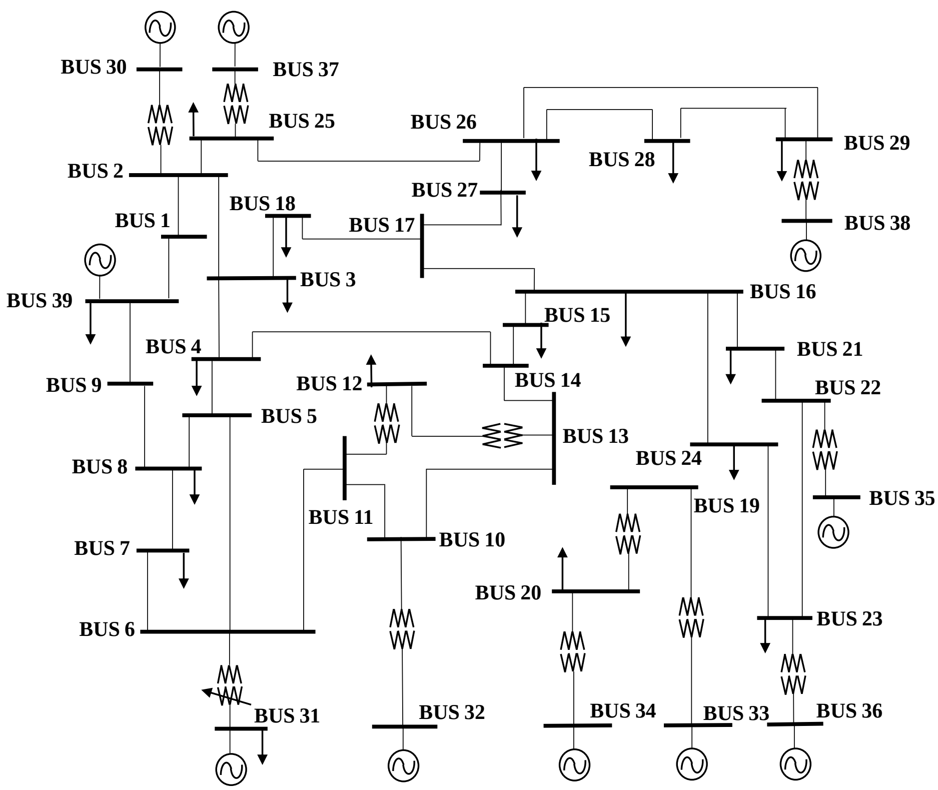

Figure A.1: A single line diagram of the IEEE 39-bus test system.

The bus data and the line data for this test system are obtained from [62] and are shown in Tables A.1 and A.2. Data for the governor parameters F_i, K_i and R_i are generated using Gaussian distributions [56] with parameters as shown in Table A.3. The values for the governor time constant T_R and the load damping constant D are assumed to be 8 and 2 respectively. In addition, reliability data for the generators are also used for this system in Chapter 2 and are shown in Table A.4.

Table A.1: Bus data for IEEE 39-bus test system.

Bus No.	Type	Demand (MW)
1	PQ	97.6
2	PQ	0
3	PQ	322
4	PQ	500
5	PQ	0
6	PQ	0
7	PQ	233.8
8	PQ	522
9	PQ	6.5
10	PQ	0
11	PQ	0
12	PQ	8.53
13	PQ	0
14	PQ	0
15	PQ	320
16	PQ	329
17	PQ	0
18	PQ	158
19	PQ	0
20	PQ	680
21	PQ	274
22	PQ	0
23	PQ	247.5
24	PQ	308.6
25	PQ	224
26	PQ	139
27	PQ	281
28	PQ	206
29	PQ	283.5
30	PV	0
31	slack	9.2
32	PV	0
33	PV	0
34	PV	0
35	PV	0
36	PV	0
37	PV	0
38	PV	0
39	PV	1104

Table A.2: Line data for IEEE 39 bus test system.

From Bus	To Bus	R (p.u.)	X (p.u.)	B (p.u.)	Transformer Tap Ratio	Line Limits (MVA)
1	2	0.0035	0.0411	0.6987	1	600
1	39	0.001	0.025	0.75	1	1000
2	3	0.0013	0.0151	0.2572	1	500
2	25	0.007	0.0086	0.146	1	500
2	30	0	0.0181	0	1.025	2500
3	4	0.0013	0.0213	0.2214	1	500
3	18	0.0011	0.0133	0.2138	1	500
4	5	0.0008	0.0128	0.1342	1	600
4	14	0.0008	0.0129	0.1382	1	500
5	6	0.0002	0.0026	0.0434	1	1200
5	8	0.0008	0.0112	0.1476	1	900
6	7	0.0006	0.0092	0.113	1	900
6	11	0.0007	0.0082	0.1389	1	480
6	31	0	0.025	0	1.07	1800
7	8	0.0004	0.0046	0.078	1	900
8	9	0.0023	0.0363	0.3804	1	900
9	39	0.001	0.025	1.2	1	900
10	11	0.0004	0.0043	0.0729	1	600
10	13	0.0004	0.0043	0.0729	1	600
10	32	0	0.02	0	1.07	2500
12	11	0.0016	0.0435	0	1.006	500
12	13	0.0016	0.0435	0	1.006	500
13	14	0.0009	0.0101	0.1723	1	600
14	15	0.0018	0.0217	0.366	1	600
15	16	0.0009	0.0094	0.171	1	600
16	17	0.0007	0.0089	0.1342	1	600
16	19	0.0016	0.0195	0.304	1	600
16	21	0.0008	0.0135	0.2548	1	600
16	24	0.0003	0.0059	0.068	1	600
17	18	0.0007	0.0082	0.1319	1	600
17	27	0.0013	0.0173	0.3216	1	600
19	20	0.0007	0.0138	0	1.06	900
19	33	0.0007	0.0142	0	1.07	900
20	34	0.0009	0.018	0	1.009	900
21	22	0.0008	0.014	0.2565	1	900
22	23	0.0006	0.0096	0.1846	1	600
22	35	0	0.0143	0	1.025	2500
23	24	0.0022	0.035	0.361	1	600
23	36	0.0005	0.0272	0	1	900
25	26	0.0032	0.0323	0.531	1	600
25	37	0.0006	0.0232	0	1.025	900
26	27	0.0014	0.0147	0.2396	1	600
26	28	0.0043	0.0474	0.7802	1	600
26	29	0.0057	0.0625	1.029	1	600
28	29	0.0014	0.0151	0.249	1	600
29	38	0.0008	0.0156	0	1.025	1200

Table A.3: Data for governor parameters.

Parameter	F_i	K_i	R_i
μ	0.25	1	0.04
σ	0.05	0.025	0.01

Table A.4: Generator data for IEEE 39-bus test system.

Unit No.	Unit Type	Capacity (MW)	Inertia (s)	Forced Outage Rate
1	Interconnection	1040	500	0.0891
2	Nuclear	646	30.3	0.0159
3	Nuclear	725	35.8	0.0159
4	Fossil	652	38.6	0.0773
5	Fossil	508	26	0.0882
6	Nuclear	687	34.8	0.0159
7	Fossil	580	26.4	0.0882
8	Nuclear	564	24.3	0.0159
9	Nuclear	865	34.5	0.0166
10	Hydro	1100	42	0.0465

APPENDIX B

IEEE RELIABILITY TEST SYSTEM

This section provides the data used for the IEEE Reliability Test System (RTS), along with a single line diagram, as shown in Fig. B.1. This test system has been used in Chapters 3 and 5 of this thesis. All data for this system are obtained from [64]. The bus data and line data are shown in Tables B.1 and B.2.

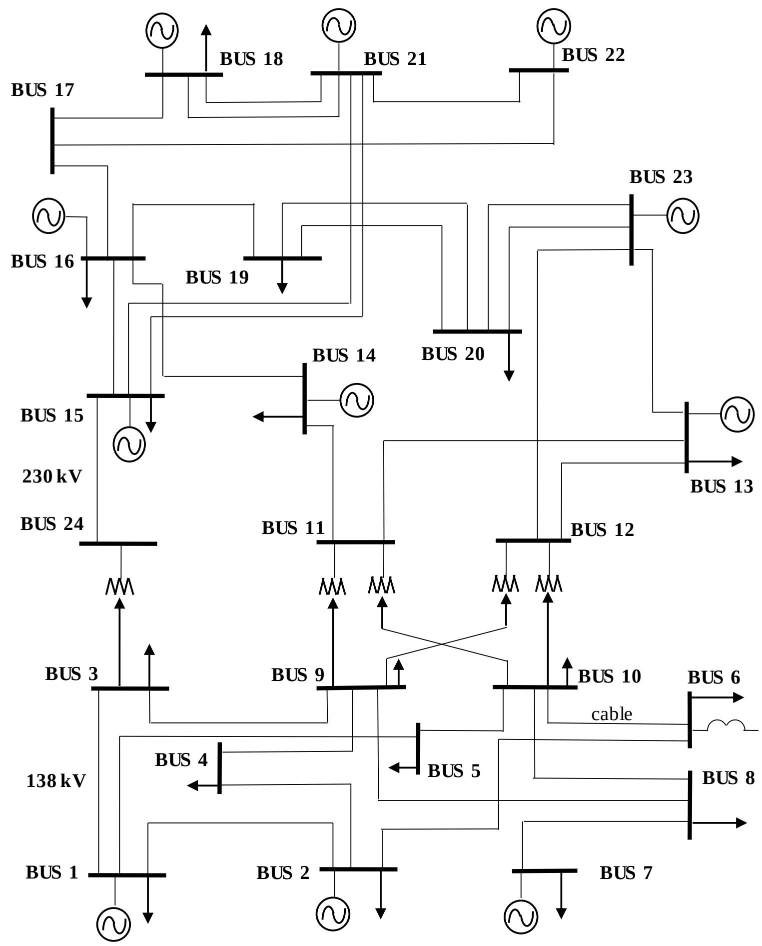

Figure B.1: A single line diagram of the IEEE Reliability Test System.

Table B.1: Bus data for the IEEE RTS.

Bus No.	Type	Demand (MW)
1	PV	108
2	PV	97
3	PQ	180
4	PQ	74
5	PQ	71
6	PQ	136
7	PV	125
8	PQ	171
9	PQ	175
10	PQ	195
11	PQ	0
12	PQ	0
13	slack	265
14	PV	194
15	PV	317
16	PV	100
17	PQ	0
18	PV	333
19	PQ	181
20	PQ	128
21	PV	0
22	PV	0
23	PV	0
24	PV	0

Table B.2: Line data for the IEEE RTS.

From Bus	To Bus	R (p.u.)	X (p.u.)	B (p.u.)	Transformer Tap Ratio	Line Limits (MVA)
1	2	0.0026	0.0139	0.4611	1	175
1	3	0.0546	0.2112	0.0572	1	175
1	5	0.0218	0.0845	0.0229	1	175
2	4	0.0328	0.1267	0.0343	1	175
2	6	0.0497	0.192	0.052	1	175
3	9	0.0308	0.119	0.0322	1	175
3	24	0.0023	0.0839	0	1.03	400
4	9	0.0268	0.1037	0.0281	1	175
5	10	0.0228	0.0883	0.0239	1	175
6	10	0.0139	0.0605	2.459	1	175
7	8	0.0159	0.0614	0.0166	1	175
8	9	0.0427	0.1651	0.0447	1	175
8	10	0.0427	0.1651	0.0447	1	175
9	11	0.0023	0.0839	0	1.03	400
9	12	0.0023	0.0839	0	1.03	400
10	11	0.0023	0.0839	0	1.02	400
10	12	0.0023	0.0839	0	1.02	400
11	13	0.0061	0.0476	0.0999	1	500
11	14	0.0054	0.0418	0.0879	1	500
12	13	0.0061	0.0476	0.0999	1	500
12	23	0.0124	0.0966	0.203	1	500
13	23	0.0111	0.0865	0.1818	1	500
14	16	0.005	0.0389	0.0818	1	500
15	16	0.0022	0.0173	0.0364	1	500
15	21	0.0063	0.049	0.103	1	500
15	21	0.0063	0.049	0.103	1	500
15	24	0.0067	0.0519	0.1091	1	500
16	17	0.0033	0.0259	0.0545	1	500
16	19	0.003	0.0231	0.0485	1	500
17	18	0.0018	0.0144	0.0303	1	500
17	22	0.0135	0.1053	0.2212	1	500
18	21	0.0033	0.0259	0.0545	1	500
18	21	0.0033	0.0259	0.0545	1	500
19	20	0.0051	0.0396	0.0833	1	500
19	20	0.0051	0.0396	0.0833	1	500
20	23	0.0028	0.0216	0.0455	1	500
20	23	0.0028	0.0216	0.0455	1	500
21	22	0.0087	0.0678	0.1424	1	500

BIBLIOGRAPHY

BIBLIOGRAPHY

[1] Renewables 2020. Technical report, International Energy Agency, 2020.

[2] U.S. Wind Industry Quarterly Market Report. Technical report, American Wind Energy Association, 2019.

[3] Benjamin Kroposki, Brian Johnson, Yingchen Zhang, Vahan Gevorgian, Paul Denholm, Bri-Mathias Hodge, and Bryan Hannegan. Achieving a 100% renewable grid: Operating electric power systems with extremely high levels of variable renewable energy. *IEEE Power and Energy Magazine*, 15(2):61–73, 2017.

[4] Ruifeng Yan, Tapan Kumar Saha, Nilesh Modi, Nahid-Al Masood, and Mehdi Mosadeghy. The combined effects of high penetration of wind and PV on power system frequency response. *Applied Energy*, 145:320–330, 2015.

[5] Nga Nguyen and Joydeep Mitra. An analysis of the effects and dependency of wind power penetration on system frequency regulation. *IEEE Trans. Sustain. Energy*, 7(1):354–363, 2015.

[6] Nga Nguyen and Joydeep Mitra. Reliability of power system with high wind penetration under frequency stability constraint. *IEEE Trans. Power Syst.*, 33(1):985–994, Jan 2018.

[7] Electric Reliability Council of Texas (ERCOT). Future Ancillary Services in ERCOT. http://www.ercot.com/content/news/presentations/2014/ERCOT_AS_Concept_Paper_Version_1.1_as_of_11-01-13_1445_black.pdf. Accessed: 2021-01-08.

[8] North American Electric Reliability Corporation. NERC IVGTF Task Report 2.4: Operating practices, procedures and tools, March 2011.

[9] Hans-Peter Beck and Ralf Hesse. Virtual synchronous machine. In *2007 9th International Conference on Electrical Power Quality and Utilisation*, pages 1–6. IEEE, 2007.

[10] Johan Driesen and Klaas Visscher. Virtual synchronous generators. In *2008 IEEE Power and Energy Society General Meeting - Conversion and Delivery of Electrical Energy in the 21st Century*, pages 1–3, July 2008.

[11] Mohammed Benidris and Joydeep Mitra. Enhancing stability performance of renewable energy generators by utilizing virtual inertia. In *2012 IEEE Power and Energy Society General Meeting*, pages 1–6. IEEE, 2012.

[12] Robert Eriksson, Niklas Modig, and Katherine Elkington. Synthetic inertia versus fast frequency response: a definition. *IET Renewable Power Generation*, 12(5):507–514, 2017.

[13] Ujjwol Tamrakar, Dipesh Shrestha, Manisha Maharjan, Bishnu P Bhattarai, Timothy M Hansen, and Reinaldo Tonkoski. Virtual inertia: Current trends and future directions. *Applied Sciences*, 7(7):654, 2017.

[14] Gauthier Delille, Bruno Francois, and Gilles Malarange. Dynamic frequency control support by energy storage to reduce the impact of wind and solar generation on isolated power system's inertia. *IEEE Trans. Sustain. Energy*, 3(4):931–939, 2012.

[15] Qing-Chang Zhong. Virtual synchronous machines: A unified interface for grid integration. *IEEE Power Electronics Magazine*, 3(4):18–27, 2016.

[16] Vaclav Knap, Sanjay K Chaudhary, Daniel-Ioan Stroe, Maciej Swierczynski, Bogdan-Ionut Craciun, and Remus Teodorescu. Sizing of an energy storage system for grid inertial response and primary frequency reserve. *IEEE Trans. Power Syst.*, 31(5):3447–3456, 2015.

[17] Meng Yue and Xiaoyu Wang. Grid inertial response-based probabilistic determination of energy storage system capacity under high solar penetration. *IEEE Trans. Sustain. Energy*, 6(3):1039–1049, 2014.

[18] Atri Bera, Michael Abdelmalak, Saad Alzahrani, Mohammed Benidris, and Joydeep Mitra. Sizing of energy storage systems for grid inertial response. In *2020 IEEE Power and Energy Society General Meeting*, pages 1–5, Aug. 2020.

[19] Hêmin Golpîra, Azin Atarodi, Shiva Amini, Arturo Román Messina, Bruno Francois, and Hassan Bevrani. Optimal energy storage system-based virtual inertia placement: A frequency stability point of view. *IEEE Trans. Power Syst.*, 35(6):4824–4835, 2020.

[20] Nga Nguyen, Mohammed Benidris, and Joydeep Mitra. A unified analysis of the impacts of stochasticity and low inertia of wind generation. In *2016 International Conference on Probabilistic Methods Applied to Power Systems (PMAPS)*, pages 1–7. IEEE, 2016.

[21] Yuri V Makarov, Clyde Loutan, Jian Ma, and Phillip De Mello. Operational impacts of wind generation on california power systems. *IEEE Trans. Power Syst.*, 24(2):1039–1050, 2009.

[22] J Charles Smith, Michael R Milligan, Edgar A DeMeo, and Brian Parsons. Utility wind integration and operating impact state of the art. *IEEE Trans. Power Syst.*, 22(3):900–908, 2007.

[23] Roy Billinton and B. Bagen. Incorporating well-being considerations in generating systems using energy storage. *IEEE Trans. Energy Convers.*, 20(1):225–230, 2005.

[24] Mary Black and Goran Strbac. Value of bulk energy storage for managing wind power fluctuations. *IEEE Trans. Energy Convers.*, 22(1):197–205, 2007.

[25] Po Hu, Rajesh Karki, and Roy Billinton. Reliability evaluation of generating systems containing wind power and energy storage. *IET generation, transmission & distribution*, 3(8):783–791, 2009.

[26] George Caralis and Arthouros Zervos. Value of wind energy on the reliability of autonomous power systems. *IET Renewable Power Generation*, 4(2):186–197, 2010.

[27] Joydeep Mitra. Reliability-based sizing of backup storage. *IEEE Trans. Power Syst.*, 25(2):1198–1199, 2010.

[28] Samer Sulaeman, Yuting Tian, Mohammed Benidris, and Joydeep Mitra. Quantification of storage necessary to firm up wind generation. *IEEE Trans. Ind. Appl.*, 53(4):3228–3236, July 2017.

[29] Nga Nguyen, Atri Bera, and Joydeep Mitra. Energy storage to improve reliability of wind integrated systems under frequency security constraint. *IEEE Trans. Ind. Appl.*, 54(5):4039–4047, Sept 2018.

[30] US Department of Energy. 20% wind energy by 2030: Increasing wind energy's contribution to US electricity supply. *Energy Efficiency and Renewable Energy Tech. Rep. DOE/GO*, pages 102008–2567, 2008.

[31] EnerNex Corporation. Eastern wind integration and transmission study. Technical report, The National Renewable Energy Lab.(NREL), 2011.

[32] GE Energy. Western wind and solar integration study. Technical report, The National Renewable Energy Lab.(NREL), 2010.

[33] Jay Apt and Paulina Jaramillo. Variable renewable energy and the electricity grid. 2014.

[34] Cristina L Archer and Mark Z Jacobson. Supplying baseload power and reducing transmission requirements by interconnecting wind farms. *Journal of Applied Meteorology and Climatology*, 46(11):1701–1717, 2007.

[35] Yannick Degeilh and Chanan Singh. A quantitative approach to wind farm diversification and reliability. *International Journal of Electrical Power & Energy Systems*, 33(2):303–314, 2011.

[36] Joshua Novacheck and Jeremiah X Johnson. Diversifying wind power in real power systems. *Renewable Energy*, 106:177–185, 2017.

[37] Francois Vallee, Jacques Lobry, and Olivier Deblecker. System reliability assessment method for wind power integration. *IEEE Trans. Power Syst.*, 23(3):1288–1297, 2008.

[38] Yih-huei Wan, Michael Milligan, and Brian Parsons. Output power correlation between adjacent wind power plants. *J. Sol. Energy Eng.*, 125(4):551–555, 2003.

[39] Abigail Krich and M Milligan. Impact of wind energy on hourly load following requirements: an hourly and seasonal analysis. Technical report, National Renewable Energy Lab., Golden, CO (US), 2005.

[40] Antonio J Conejo, Miguel Carrión, Juan M Morales, et al. *Decision making under uncertainty in electricity markets*, volume 1. Springer, 2010.

[41] Federal Energy Regulatory Commission. Electric Power Markets. https://www.ferc.gov/market-assessments/mkt-electric/overview.asp. [Online; accessed 15-May-2020].

[42] Raymond H Byrne, Tu A Nguyen, David A Copp, Babu R Chalamala, and Imre Gyuk. Energy management and optimization methods for grid energy storage systems. *IEEE Access*, 6:13231–13260, 2017.

[43] Rahul Walawalkar, Jay Apt, and Rick Mancini. Economics of electric energy storage for energy arbitrage and regulation in New York. *Energy Policy*, 35(4):2558 – 2568, 2007.

[44] Yuting Tian, Atri Bera, Mohammed Benidris, and Joydeep Mitra. Stacked revenue and technical benefits of a grid-connected energy storage system. *IEEE Trans. Ind. Appl.*, 54(4):3034–3043, July 2018.

[45] Tu A. Nguyen, Raymond H. Byrne, Ricky J. Concepcion, and Imre Gyuk. Maximizing revenue from electrical energy storage in MISO energy and frequency regulation markets. In *2017 IEEE Power Energy Society General Meeting*, pages 1–5, July 2017.

[46] Robert R Booth. Power system simulation model based on probability analysis. *IEEE Trans. Power App. Syst.*, (1):62–69, 1972.

[47] Chanan Singh, Panida Jirutitijaroen, and Joydeep Mitra. *Electric Power Grid Reliability Evaluation: Models and Methods*. John Wiley & Sons, Hoboken, NJ, 2019.

[48] KF Schenk, RB Misra, S Vassos, and W Wen. A new method for the evaluation of expected energy generation and loss of load probability. *IEEE Trans. Power App. Syst.*, (2):294–303, 1984.

[49] Q Ahsan, KF Schenk, and RB Misra. Expected energy production cost of two interconnected systems with correlated demands. *IEEE Trans. Power App. Syst.*, (7):2155–2164, 1983.

[50] Andrew Keane, Michael Milligan, Chris J Dent, Bernhard Hasche, Claudine D'Annunzio, Ken Dragoon, Hannele Holttinen, Nader Samaan, Lennart Soder, and Mark O'Malley. Capacity value of wind power. *IEEE Transactions on Power Systems*, 26(2):564–572, 2010.

[51] F Castro Sayas and RN Allan. Generation availability assessment of wind farms. *IEE Proceedings-Generation, Transmission and Distribution*, 143(5):507–518, 1996.

[52] Roy Billinton and Guang Bai. Generating capacity adequacy associated with wind energy. *IEEE Trans. Energy Convers.*, 19(3):641–646, 2004.

[53] Hassan Bevrani. Real power compensation and frequency control. *Robust Power System Frequency Control*, pages 1–23, 2009.

[54] Peter W Sauer and Mangalore Anantha Pai. *Power System Dynamics and Stability*, volume 101. Prentice Hall Upper Saddle River, NJ, 1998.

[55] Vijay Vittal, James D McCalley, Paul M Anderson, and AA Fouad. *Power System Control and Stability*. John Wiley & Sons, 2019.

[56] Hamed Ahmadi and Hassan Ghasemi. Security-constrained unit commitment with linearized system frequency limit constraints. *IEEE Trans. Power Syst.*, 29(4):1536–1545, 2014.

[57] Nga Nguyen, Saleh Almasabi, Atri Bera, and Joydeep Mitra. Optimal power flow incorporating frequency security constraint. *IEEE Trans. Ind. Appl.*, 55(6):6508–6516, 2019.

[58] Nga Nguyen, Atri Bera, and Joydeep Mitra. Energy storage to improve reliability of wind integrated systems under frequency security constraint. *IEEE Trans. Ind Appl.*, 54(5):4039–4047, 2018.

[59] Joseph H Eto, John Undrill, Ciaran Roberts, Peter Mackin, and Jeffrey Ellis. 2018 LBNL frequency control requirements for reliable interconnection frequency response. 2018.

[60] North American Electric Reliability Corporation. Fast Frequency Response Concepts and Bulk Power System Reliability Needs, March 2020.

[61] North American Electric Reliability Corporation. Standard PRC-006 — Automatic Underfrequency Load Shedding, 2014.

[62] T Athay, R Podmore, and S Virmani. A practical method for the direct analysis of transient stability. *IEEE Trans. Power Appar. Syst.*, (2):573–584, 1979.

[63] The Wind Prospector. https://maps.nrel.gov/wind-prospector/. Accessed: 2021-03-23.

[64] Reliability Test System Task Force of the Application of Probability Methods Subcommittee. IEEE Reliability Test System. *IEEE Trans. Power Appar. Syst.*, PAS-98(6):2047–2054, Nov. 1979.

[65] North American Electric Reliability Corporation. Generating Availability Data System (GADS). https://www.nerc.com/pa/RAPA/gads/Pages/Reports.aspx. Accessed: 2020-08-22.

[66] Huajie Ding, Pierre Pinson, Zechun Hu, Jianhui Wang, and Yonghua Song. Optimal offering and operating strategy for a large wind-storage system as a price maker. *IEEE Trans. Power Syst.*, 32(6):4904–4913, 2017.

[67] Bolong Cheng and Warren B Powell. Co-optimizing battery storage for the frequency regulation and energy arbitrage using multi-scale dynamic programming. *IEEE Transactions on Smart Grid*, 9(3):1997–2005, 2016.

[68] Xiaohe Yan, Chenghong Gu, Heather Wyman-Pain, and Furong Li. Capacity share optimization for multiservice energy storage management under portfolio theory. *IEEE Trans. on Ind. Electron.*, 66(2):1598–1607, 2018.

[69] Jim Eyer and Garth Corey. Energy storage for the electricity grid: Benefits and market potential assessment guide. *Sandia National Laboratories*, 20(10):5, 2010.

[70] Bruce Dunn, Haresh Kamath, and Jean-Marie Tarascon. Electrical energy storage for the grid: a battery of choices. *Science*, 334(6058):928–935, 2011.

[71] U.S. Energy Information Administration. U.S. Battery Storage Market Trends, 2018.

[72] Monitoring Analytics, LLC. State of the Market Report for PJM, 2018.

[73] Scott B. Peterson, Jay Apt, and J.F. Whitacre. Lithium-ion battery cell degradation resulting from realistic vehicle and vehicle-to-grid utilization. *Journal of Power Sources*, 195(8):2385 – 2392, 2010.

[74] Yuchao Qin, Haochen Hua, and Junwei Cao. Stochastic optimal control scheme for battery lifetime extension in islanded microgrid via a novel modeling approach. *IEEE Trans. Smart Grid*, 10(4):4467–4475, 2018.

[75] Chengquan Ju and Peng Wang. Energy management system for microgrids including batteries with degradation costs. In *2016 IEEE International Conference on Power System Technology (POWERCON)*, pages 1–6. IEEE, 2016.

[76] Chunyang Liu, Xiuli Wang, Xiong Wu, and Jingli Guo. Economic scheduling model of microgrid considering the lifetime of batteries. *IET Generation, Transmission & Distribution*, 11(3):759–767, 2017.

[77] Bolun Xu, Jinye Zhao, Tongxin Zheng, Eugene Litvinov, and Daniel S Kirschen. Factoring the cycle aging cost of batteries participating in electricity markets. *IEEE Transactions on Power Systems*, 33(2):2248–2259, 2017.

[78] Stephen D Downing and DF Socie. Simple rainflow counting algorithms. *International Journal of Fatigue*, 4(1):31–40, Jan. 1982.

[79] National Renewable Energy Laboratory. Declining Renewable Costs Drive Focus on Energy Storage. https://www.nrel.gov/news/features/2020/declining-renewable-costs-drive-focus-on-energy-storage.html. [Online; accessed 15-May-2020].

[80] Atri Bera, Saleh Almasabi, Joydeep Mitra, Babu Chalamala, and Raymond H. Byrne. Spatiotemporal optimization of grid-connected energy storage to maximize economic benefits. In *2019 IEEE Industry Applications Society Annual Meeting (IAS)*, pages 1–7, Oct. 2019.

[81] North American Electric Reliability Corporation. *Operating practices, procedures and tools*. North American Electric Reliability Corporation, Princeton, NJ, Mar. 2011.

[82] Federal Energy Regulatory Commission. Final rule order no. 755: Frequency regulation compensation in the organized wholesale power markets. 137, October 2011.

[83] PJM. Manual 28: Operating agreement accounting, 2014.

[84] Olivia Leitermann. *Energy storage for frequency regulation on the electric grid*. PhD thesis, Massachusetts Institute of Technology, 2012.

[85] Bolun Xu, Alexandre Oudalov, Andreas Ulbig, Göran Andersson, and Daniel S Kirschen. Modeling of lithium-ion battery degradation for cell life assessment. *IEEE Transactions on Smart Grid*, 9(2):1131–1140, 2016.

[86] Erin Cready, John Lippert, Josh Pihl, Irwin Weinstock, Phillip Symons, and Rudolph G Jungst. Final report technical and economic feasibility of applying used EV batteries in stationary applications. *Sandia National Laboratory*, 2003.

[87] Leila Ahmadi, Michael Fowler, Steven B. Young, Roydon A. Fraser, Ben Gaffney, and Sean B. Walker. Energy efficiency of li-ion battery packs re-used in stationary power applications. *Sustainable Energy Technologies and Assessments*, 8:9 – 17, 2014.

[88] Gillian Lacey, Ghamin Putrus, and Anwar Salim. The use of second life electric vehicle batteries for grid support. In *Eurocon 2013*, pages 1255–1261. IEEE, 2013.

[89] Lluc Canals Casals, Mattia Barbero, and Cristina Corchero. Reused second life batteries for aggregated demand response services. *Journal of Cleaner Production*, 212:99 – 108, 2019.

[90] Willett Kempton and Jasna Tomić. Vehicle-to-grid power fundamentals: Calculating capacity and net revenue. *Journal of Power Sources*, 144(1):268–279, 2005.

[91] PJM. RTO Regulation Signal Data, 2018.

[92] Raymond H Byrne and Cesar Augusto Silva-Monroy. Estimating the maximum potential revenue for grid connected electricity storage: Arbitrage and regulation. *Sandia National Laboratories*, 2012.

[93] Atri Bera, Joydeep Mitra, and Nga Nguyen. Lifetime revenue from energy storage considering battery degradation. In *2019 North American Power Symposium (NAPS)*, pages 1–6, 2019.

[94] Yuting Tian, Dongbo Zhao, Tianqi Hong, and Bai Cui. Cost and efficiency analysis for hybrid ac/dc distribution system planning with pv and battery. In *2020 IEEE Power & Energy Society Innovative Smart Grid Technologies Conference (ISGT)*, pages 1–5. IEEE, 2020.

[95] Susan M Schoenung and William V Hassenzahl. Long-vs. short-term energy storage technologies analysis: a life-cycle cost study: a study for the DOE energy storage systems program. Technical report, Sandia National Laboratories, 2003.

[96] PJM. PJM Data Miner2.

[97] Ran Fu, Timothy W Remo, and Robert M Margolis. 2018 US utility-scale photovoltaics-plus-energy storage system costs benchmark. Technical report, National Renewable Energy Lab.(NREL), Golden, CO (United States), 2018.

[98] Wesley J Cole and Allister Frazier. Cost projections for utility-scale battery storage. Technical report, National Renewable Energy Lab. (NREL), Golden, CO (United States), 2019.

[99] Nicholas DiOrio, Aron Dobos, and Steven Janzou. Economic analysis case studies of battery energy storage with sam. Technical report, National Renewable Energy Lab. (NREL), Golden, CO (United States), 2015.

[100] William E Hart, Jean-Paul Watson, and David L Woodruff. Pyomo: modeling and solving mathematical programs in python. *Mathematical Programming Computation*, 3(3):219–260, 2011.

[101] California ISO. Flexible ramping product. http://www.caiso.com/informed/Pages/StakeholderProcesses/CompletedClosedStakeholderInitiatives/FlexibleRampingProduct.aspx. Accessed: 2020-08-22.

[102] Jonathan Brisebois and Noël Aubut. Wind farm inertia emulation to fulfill Hydro-Québec's specific need. In *2011 IEEE Power and Energy Society General Meeting*, pages 1–7. IEEE, 2011.

[103] Weifeng Li, Pengwei Du, and Ning Lu. Design of a new primary frequency control market for hosting frequency response reserve offers from both generators and loads. *IEEE Trans. Smart Grid*, 9(5):4883–4892, 2017.

[104] Nimish Soni, Suryanarayana Doolla, and Mukul C Chandorkar. Improvement of transient response in microgrids using virtual inertia. *IEEE Trans. Power Del.*, 28(3):1830–1838, 2013.

[105] M. F. M. Arani and E. F. El-Saadany. Implementing virtual inertia in DFIG-based wind power generation. *IEEE Trans. Power Syst.*, 28(2):1373–1384, 2013.

[106] Gauthier Marc Aime Delille. Participation of energy storage in the advanced management of power systems: organizational, technical and economic approaches in distribution grids. 2010.

[107] Adri Junyent-Ferr, Yousef Pipelzadeh, and Tim C Green. Blending hvdc-link energy storage and offshore wind turbine inertia for fast frequency response. *IEEE Trans. Sustain. Energy*, 6(3):1059–1066, 2014.

[108] Samir M Alhejaj and Francisco M Gonzalez-Longatt. Investigation on grid-scale bess providing inertial response support. In *2016 IEEE International Conference on Power System Technology (POWERCON)*, pages 1–6. IEEE, 2016.

[109] Ju Liu, Jinyu Wen, Wei Yao, and Yao Long. Solution to short-term frequency response of wind farms by using energy storage systems. *IET Renewable Power Generation*, 10(5):669–678, 2016.

[110] Arash Anzalchi, Maneli Malek Pour, and Arif Sarwat. A combinatorial approach for addressing intermittency and providing inertial response in a grid-connected photovoltaic system. In *2016 IEEE Power and Energy Society General Meeting (PESGM)*, pages 1–5. IEEE, 2016.

[111] Julia L Higle. Stochastic programming: Optimization when uncertainty matters. In *Emerging Theory, Methods, and Applications*, pages 30–53. Informs, 2005.

[112] Roy Billinton, Hua Chen, and R Ghajar. Time-series models for reliability evaluation of power systems including wind energy. *Microelectronics Reliability*, 36(9):1253–1261, 1996.

[113] Alexander Sturt and Goran Strbac. Efficient stochastic scheduling for simulation of wind-integrated power systems. *IEEE Trans. Power Syst.*, 27(1):323–334, 2011.

[114] Paul Giorsetto and Kent F Utsurogi. Development of a new procedure for reliability modeling of wind turbine generators. *IEEE Trans. Power App. Syst.*, (1):134–143, 1983.

[115] Peng Xiong and Chanan Singh. Optimal planning of storage in power systems integrated with wind power generation. *IEEE Trans. Sustain. Energy*, 7(1):232–240, 2015.

[116] Stephan Dempe. *Bilevel optimization: theory, algorithms and applications*. TU Bergakademie Freiberg, Fakultät für Mathematik und Informatik, 2018.

[117] William Eugene Hart, Jean-Paul Watson, John Daniel Siirola, and Richard Li-Yang Chen. Modeling bilevel programs in pyomo. Technical report, Sandia National Lab.(SNL-NM), Albuquerque, NM (United States); Sandia . . . , 2016.

[118] David M Rosewater, David A Copp, Tu A Nguyen, Raymond H Byrne, and Surya Santoso. Battery energy storage models for optimal control. *IEEE Access*, 7:178357–178391, 2019.

[119] US Energy Information Administration (EIA). Average Power Plant Operating Expenses for Major U.S. Investor-Owned Electric Utilities, 2009 through 2019. https://www.eia.gov/electricity/annual/html/epa_08_04.html. Accessed: 2020-11-08.

[120] Joydeep Mitra and Mallikarjuna R Vallem. Determination of storage required to meet reliability guarantees on island-capable microgrids with intermittent sources. *IEEE Trans. Power Syst.*, 27(4):2360–2367, 2012.

[121] Chanan Singh and Joydeep Mitra. Monte Carlo simulation for reliability analysis of emergency and standby power systems. In *1995 IEEE Industry Applications Conference*, volume 3, pages 2290–2295 vol.3, Oct 1995.

[122] Ronald N Allan, Roy Billinton, and NMK Abdel-Gawad. The IEEE reliability test system-extensions to and evaluation of the generating system. *IEEE Trans. Power Syst.*, 1(4):1–7, 1986.

[123] Vestas 4 MW Platform. https://www.vestas.com/en/products/4%20mw%20platform#! Accessed: 2021-03-23.

[124] Samer Sulaeman, Mohammed Benidris, Joydeep Mitra, and Chanan Singh. A wind farm reliability model considering both wind variability and turbine forced outages. *IEEE Trans. Sustain. Energy*, 8(2):629–637, April 2017.

[125] Kendall Mongird, Vilayanur V Viswanathan, Patrick J Balducci, Md Jan E Alam, Vanshika Fotedar, V S Koritarov, and Boualem Hadjerioua. Energy storage technology and cost characterization report. Technical report, Pacific Northwest National Lab.(PNNL), Richland, WA (United States), 2019.

[126] Juan Andrade and Ross Baldick. Estimation of transmission costs for new generation. *University of Texas*, 2016.